



An Investigation into Applying Polarisation to Hydrogen Surface Reactions on the Diamond (100) Reconstructed Dimer Surface Using Density Functional Theory Methods and its Effects on Computational Runtime

By James Andrews

# Contents

<b>Literature Review</b> .....	<b>1</b>
<b>Aim</b> .....	<b>1</b>
<b>Background and Context</b> .....	<b>1</b>
<b>Overview of Diamond Chemical Vapour Deposition Process</b> .....	<b>3</b>
<b>The Role of Hydrogen</b> .....	<b>4</b>
<b>Reactor Components</b> .....	<b>5</b>
<b>Computational Studies</b> .....	<b>10</b>
<b>Dimer Mechanism</b> .....	<b>13</b>
<b>Requirement for Parameter Review</b> .....	<b>20</b>
<b>Relevant Energy Barriers</b> .....	<b>20</b>
<b>Summary</b> .....	<b>21</b>
<b>Aims of the Thesis</b> .....	<b>23</b>
<b>Methodology</b> .....	<b>24</b>
<b>Basis Set Investigation</b> .....	<b>24</b>
<b>Tolerances</b> .....	<b>24</b>
<b>Functionals</b> .....	<b>25</b>
<b>Layers Determination</b> .....	<b>26</b>
<b>Model Construction</b> .....	<b>26</b>
<b>Polarisation Application</b> .....	<b>26</b>
<b>Formation of the Surface Radical</b> .....	<b>27</b>
<b>Hydrogen Scanning</b> .....	<b>27</b>
<b>Energy Barrier Calculations</b> .....	<b>28</b>
<b>B3LYP Calculations</b> .....	<b>28</b>
<b>Computational Runtime</b> .....	<b>29</b>
<b>Geometry Observations</b> .....	<b>29</b>
<b>Results and Discussion</b> .....	<b>30</b>
<b>Lattice Parameter and Basis Set Calculations</b> .....	<b>30</b>
<b>Terminated and Radical Energy Data</b> .....	<b>32</b>
<b>Hydrogen Scan Data</b> .....	<b>34</b>
<b>Energy Barrier of Hydrogen Adsorption</b> .....	<b>37</b>
<b>B3LYP Single-point Data</b> .....	<b>39</b>
<b>Computational Runtime</b> .....	<b>40</b>
<b>Functional Runtime</b> .....	<b>41</b>

<b>Geometry Observations .....</b>	<b>42</b>
<b>Terminated and C-Radical Differences.....</b>	<b>42</b>
<b>Transition State Geometry.....</b>	<b>45</b>
<b>Limitations of the Thesis .....</b>	<b>47</b>
<b>B3LYP Optimisation.....</b>	<b>48</b>
<b>Further Studies .....</b>	<b>48</b>
<b>Conclusion .....</b>	<b>49</b>
<b>References.....</b>	<b>50</b>

# Literature Review

## Aim

This literature review intends to identify the key concepts, models and theories of diamond vapour chemical deposition (CVD) which have resulted in the development of today's standards. The original intention was to critically analyse the literature in two separate sections, the first being the experimental progress carried out primarily between the 1950s up to the 1990s. The second was going to be the computational analysis of the thermodynamic and kinetic properties of the surface reactions that occur during the growth process. These studies occurred mainly during and after the 1990s. Due to much of CVD diamond progress occurring in the 1990s, the review will be based on themes rather than the year they occurred. Instead, this review will explore research concerning components of CVD diamond growth, in addition to the literature that contributed towards the understanding of the growth mechanism.

The layout of this literature review will comprise two overarching sections. The first section will contain the experimental literature that led to the refinement of the diamond chemical vapour deposition (CVD) method as well as the 1955 conception and subsequent publication in 1962 by W. G. Eversole.<sup>1</sup> The second section will focus on the computational studies that led to the understanding of the dimer growth mechanism, which overall inserts a single, gaseous carbon atom into the surface of the diamond, the first step in forming a new film. The dimer reconstruction, which will be explained below, is relevant to this thesis. This involves the energy barriers to the H adsorption and H abstraction processes.

## Background and Context

Diamond is a solid, carbon-containing crystal and in its bulk form it has a giant covalent structure with each carbon atom covalently bonded to four other carbon atoms. This creates an incredibly stable crystal lattice with a Debye temperature of 2240 K.<sup>2</sup> The surface of diamond has a different structure to that of the bulk and reconstruction takes place. Each surface carbon bonds to three other carbons and terminated by one hydrogen atom. The reconstructed form of diamond is used when investigating surface reactions,<sup>3,4</sup> with the (2x1) reconstruction being the primary theoretical structure of diamond investigated in this research.

There are several ways diamonds form naturally with most forming in the Earth's mantle about 90 miles under the surface with the aid of enormous pressures.<sup>5</sup> Geologists and miners look for the presence of diamond by searching for features in the Earth's surface that are often attributed with the presence of diamond, such as lamproite pipes.<sup>5</sup> Miners rely on these pipes to obtain diamonds as

90 miles is too deep to drill. Furthermore, diamonds can be found between oceanic and continental plates.<sup>5</sup> The process of tectonics, shifts these plates, subjecting them to increasingly greater temperatures and pressures, favourable for natural diamond growth.<sup>5</sup>

After being cut and polished, mined diamonds are commonly used as gemstones; the clarity and colour are valued most.<sup>6</sup> The importation of diamonds into the United States in 2018 totalled \$26 billion with non-diamond gemstone importations only totalling \$2 billion, highlighting the popularity of diamond as a gemstone.<sup>6</sup> In addition to gemstones, diamonds are widely used in industry mainly in cutting, drilling and polishing procedures. Hardness and thermal conductivity are sort after characteristics required for these procedures.<sup>6</sup>

Diamond is a naturally forming carbon mineral, with a huge range of properties. It is the hardest natural substance on earth;<sup>7</sup> this is thanks to its fully covalent lattice. In addition, diamond is a great thermal conductor, four times more thermally conductive than copper at room temperature, provided there are no defects in the crystal.<sup>8</sup> Gicquel et al.<sup>8</sup> in 2001, suggested diamond has potential applications as semi-conductors with the aid of doping, where impurities are purposely inserted into the diamond lattice.<sup>9</sup> Furthermore, the electrical properties of diamond allow for transparency of a range of wavelengths, spanning from UV to IR and therefore can be applied to optics,<sup>9</sup> such as infrared windows.<sup>7</sup> These properties offer diamond to many applications such as cutting tools due to their hardness and thermal stability or heat sinks in electronics due to diamond being a fantastic thermal conductor as well as having a large electrical resistance.<sup>8</sup>

In 1955, the first synthetic diamond was formed, although it was not published until 1962. It was successfully grown by placing a graphite bar under 200 kilobars of pressure and heating it to 4000 K.<sup>10</sup> Published by General Electric and headed by F. P. Bundy,<sup>10</sup> the paper described the successful growth of a diamond of 0.06 inches in diameter. Fig. 1 is a phase diagram that includes their work and previous literature showing the regions of pressure and temperature available to produce diamond. From Fig. 1, it can be seen that graphite, as well as metastable diamond, can be formed in the region of low pressure and medium to high temperatures, labelled A. Metastable means the diamond is stable as long as the conditions such as temperature and pressure are not disturbed.

Using low pressure is a far more economically viable method, due to the cost of the equipment required to produce high pressures. Therefore, research into using low-pressure methods to form new

diamonds was a very interesting avenue to explore at the time, with huge corporations such as Union Carbide interested in researching low-pressure techniques.

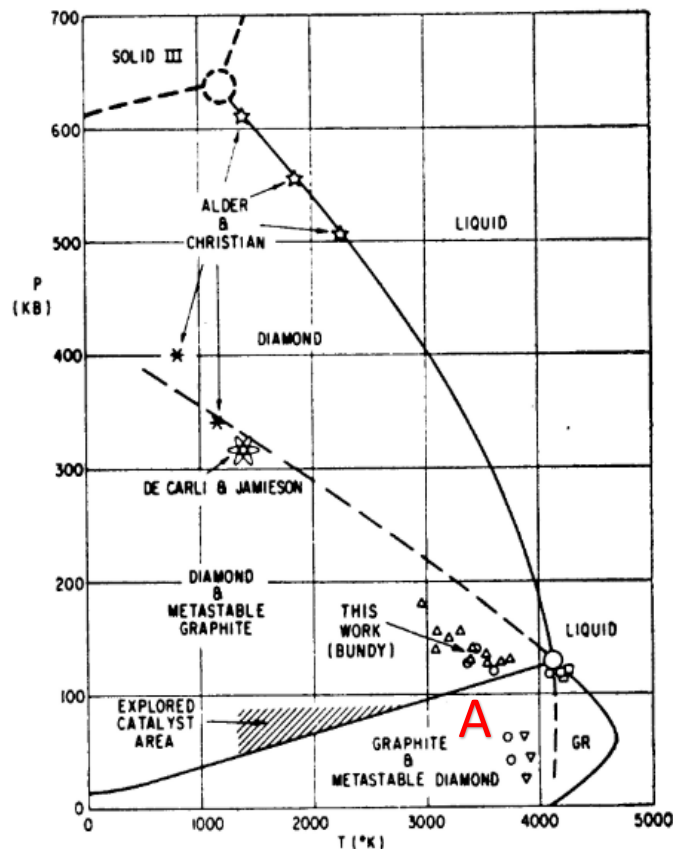


Figure 1 - Phase Diagram from F. Bundy, 1962

## Overview of Diamond Chemical Vapour Deposition Process

Diamond chemical vapour deposition (CVD) produces synthetic new diamond films from gaseous vapour specific in structure to fit a particular purpose, as the characteristics of a diamond is dependent on the structure itself. For example, polarisers require diamond films of no thicker than  $10\ \mu\text{m}$ ,<sup>8</sup> and diamond in heat sinks require high intrinsic quality<sup>8</sup> to ensure the properties needed.

Diamond CVD employs low pressures, such as  $0.09^1\ \text{atm}$ , along with medium to high temperatures, differing from nature's method of using high pressure and high temperatures. The process deposits activated carbon species onto a heated substrate with the aid of atomic hydrogen. The activated carbon species and atomic hydrogen can be formed through a range of methods, usually either a hot filament (HF) or microwave cavity (MW), which activate the gas species.

Diamond growth is made up of straightforward surface reactions. However, the actual growth of just a single diamond film is more complicated due to large number of different possibilities which can change the growth. The difficulties of ensuring that the substrate is built upon evenly are huge; with areas growing faster than others, lateral growth being slower than vertical growth, carbon defects

such as adsorption to previously adsorbed species as well as potential impurities causing defects being doped into the new film. Therefore, the task of understanding the underlying surface chemistry is important so that researchers can tailor growth conditions to avoid these issues.

Diamond CVD was first published in 1962 in a United States Patent by W. G. Eversole, working for Union Carbide.<sup>1</sup> The pioneering study described the use of natural diamond powder as a substrate with weight gains of 0.16% and 4.2% of the initial powder weight. The invention uses low pressure and temperatures between 900 and 1100 °C to achieve diamond deposition.<sup>1</sup> The patent itself is important because it showed that low-pressure conditions are capable of producing new diamond and paved the way for the next 70 years of research.

Whilst the patent is a significant breakthrough in the production of synthetic diamond, it is far from perfect when compared to today's standard. The main issue with Eversole's patent was the accumulation of black carbon on the diamond powder, which was identified by x-ray examination as graphite deposits.<sup>1</sup> This warranted cleaning stages between each growth phase, making Eversole's method a batch process, which reduced the efficiency of the growth of new diamond, with cleaning stages lasting for up to 16 hours.

The use of acid is widely quoted throughout the patent with HCl, HNO<sub>3</sub>, H<sub>2</sub>SO<sub>4</sub>, and sulphuric-chromic acid being proposed as cleaning agents, to remove undesired graphite deposits and in turn, leaving diamond crystals.<sup>1</sup> Furthermore, the cleaning processes were wildly different in duration depending on the growth process, with the patent quoting anywhere from a few minutes to one or two hundred hours.<sup>1</sup> Following Eversole's first work in the 1950s, scientists have been trying to move toward a standard mechanistic and experimental model for diamond growth under CVD conditions.

## The Role of Hydrogen

Soon after the release of Eversole's patent, research into the issues with the patent's method proceeded. The patent itself mentions the use of hydrogen as a cleaning agent, with the grown diamond removed from the reactor, and placed under a hydrogen pressure at 1000 to 1100 °C.

In 1968 Angus et al.<sup>11</sup> succeeded in building upon the cleaning phase of the diamond growth process. They carried out multiple depositions and cleaning cycles on 26 separate samples of natural diamond powder, recording the cumulative weight gain at the end of the process.<sup>11</sup>

The paper presented a reliable way of removing graphite through the use of H<sub>2</sub> at high pressures (50 atm) along with high temperatures (1033 °C) for seven hours.<sup>11</sup> The experiment was set up to ensure 99.90% of graphite was removed,<sup>11</sup> with the rates of reactions calculated using expressions from a previous paper on graphitic etching using hydrogen by Heddon.<sup>11</sup> Heddon carried out etching

experiments upon graphite, which led to etching of 99.99%. These rates calculated by Angus et al. could be questioned, as they are applying etching rates of graphite in its microstructure, whilst they are etching bulk graphite from the diamond's surface.

In 1966, shortly before Angus et al.'s paper was published, Lander and Morrison<sup>12</sup> observed the structure of the diamond's surface using low energy electron diffraction.<sup>12</sup> The authors found that H<sub>2</sub> ensured the diamond kept the reconstructed surface, which is required for diamond growth to occur.<sup>12</sup> Furthermore, they showed that the reconstruction could be maintained using low-pressure H<sub>2</sub> along with 1000 °C, showing hydrogen has multiple roles in the CVD process.<sup>12</sup>

After the experimental research of the 80s, the role of hydrogen became much more understood by the time the 1990s commenced. In 1989, a paper by Belton and Schmiegel<sup>13</sup> described experiments carried out in order to understand the states of surface carbon during the growth process. By using a growth reactor with a 0.5% CH<sub>4</sub> in H<sub>2</sub> gas mixture they grew a diamond on scratched and unscratched foils of Pt which were then analysed using x-ray photoelectron spectroscopy.<sup>13</sup> They concluded that H played a key role in ensuring surface concentration and stability of adsorbed hydrocarbons such as CH<sub>4</sub>. Hydrogen is in a dynamic equilibrium, simultaneously adsorbing to and abstracting hydrogen from the surface, producing and terminating carbon radicals on the film, and therefore high H concentrations are required for diamond CVD.<sup>4,13</sup>

In 2005, Netto et al.<sup>14</sup> published further conclusions to support the need for high concentrations of H<sub>2</sub>. They carried out simulations using a range of H concentrations, with the highest being 10<sup>-7</sup> mol cm<sup>3</sup> and the lowest as 10<sup>-11</sup> mol cm<sup>3</sup>. The average growth rates for both were 4.95 and 0.043 μm hr<sup>-1</sup> respectively.<sup>14</sup> This shows that the highest concentration produced the highest growth rates, as the H is activating the diamond's surface via the methods described above.

## Reactor Components

### Activation Method

The activation of the gas mixture is key to efficient diamond growth as it forms the activated species that facilitate the deposition of new carbon to the substrate. Eversole did not specify an activation method specifically, with the reactor being heated between 900 to 1000 °C, which may be deemed to activate the growth species.

Today, the most common methods for activation are the hot filament (HF), see Fig. 2 and microwaves (MW), see Fig. 3. However, there has been research into the use of radio frequencies (RF) also.<sup>15-18</sup>

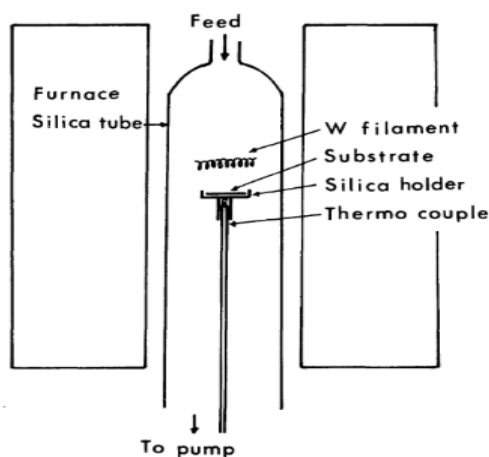


Figure 2 - Extract from Matsumoto et al. - Diagram of Hot Filament Reactor

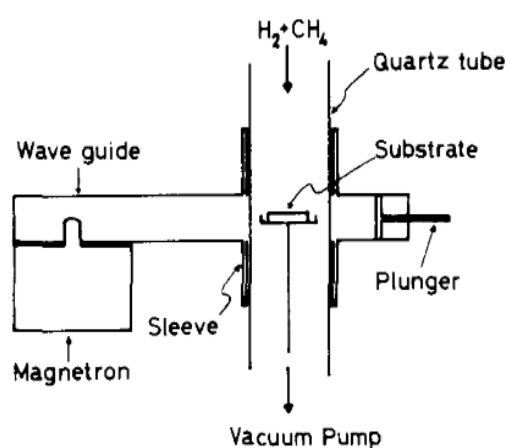


Figure 3 - Extract from Kamo et al. - Diagram of Hot Filament Reactor

In the early 80s, the Japanese National Institute for Research in Inorganic Materials (NIRIM) published a series of papers reporting their research concerning the activation method and substrate as well as making conclusions on the gas mixtures used in diamond CVD.

This highlighted the breadth of the studies undertaken by the Japanese group. The group attempted to tackle the low growth rates published in previous literature<sup>1</sup> and set up their experiment similar to previous literature,<sup>1,11</sup> as seen in Fig. 2 and 3.

Matsumoto et al.<sup>19</sup> observed that the use of low percentage CH<sub>4</sub> had a very slow deposition rate, and found that the use of a hot filament greatly increased the rate of deposition of CH<sub>4</sub> onto the surface of the substrate. In terms of the activation method, they used a heated tungsten filament and found that diamond growth rates increased with temperature of the filament.<sup>19</sup> They concluded that the filament decomposes the H<sub>2</sub> into H radicals which in turn facilitate the formation of the activated hydrocarbon growth species. The activated hydrocarbon species are formed through reactions between atomic H and gaseous CH<sub>4</sub>. Kang and Musgrave<sup>20</sup> cite the activation energy for this process to be 37.7 kJ mol<sup>-1</sup>. This is an area that Eversole and Angus et al. do not refer to and hence is a limitation of earlier literature.<sup>1,11</sup>

Furthermore, NIRIM investigated the changes that different variables have on diamond growth, such as filament temperature, reagent concentration and flow rate. However, at higher concentrations of CH<sub>4</sub> with high filament temperatures increased graphite deposition was observed, concluding that these were unfavourable conditions for diamond growth.<sup>19</sup>

In addition, the paper observed the impact of the filament-substrate distance on growth.<sup>19</sup> Whilst most experiments cited in the paper had a distance of 10 mm between the filament and the substrate, it was found that growth rate decreased as the distance between the two components increased. This

indicated that hot filaments worked most efficiently when the distance between the filament and the substrate were as small as possible, whilst not in direct contact.<sup>19</sup> It is recognised that studies following this, did not identify this parameter as being an area for change due to the fact it is rarely mentioned. This suggests that later studies were satisfied with the measurement of 10 mm.

Having realised that the activation of carbon species was required for diamond growth, NIRIM looked toward new activation methods. The use of microwaves was researched and published in 1983, where they used a magnetron to emit microwaves at 2.45GHz, using a power supply of 300 – 700 W.<sup>17</sup> They continued to use hydrogen and methane as the gas mixture along with temperatures of 800 – 1000 °C. This slightly lower than previous literature.<sup>1,11</sup> By analysing the films using Raman spectroscopy and electron diffraction,<sup>17</sup> Kamo et al. found microwaves were effective in growing diamond films with the (111) and (100) faces predominantly forming.<sup>17</sup> They achieved growth rates of 3  $\mu\text{m hr}^{-1}$  improving upon previous growth rates of 1  $\mu\text{m hr}^{-1}$  in 1982.<sup>17,18</sup>

By 2000, May<sup>15</sup> explained the rate of growth in microwave reactors is heavily influenced by the power supply to the microwave emitted, with 5 kW producing growth rates of 10  $\mu\text{m hr}^{-1}$ . Whereas the NIRIM group cited rates of 3  $\mu\text{m hr}^{-1}$  with 300 – 700 W of power. May also provided a rationale for the growth rates being dependent on the power supply; microwaves more efficiently form the radical species, increasing the concentration of H and CH<sub>3</sub> in the gas phase which then facilitate growth upon the substrate.<sup>15</sup>

Research on using radio frequencies (RF) to activate the growth species was carried out in 1985. Matsumoto et al.<sup>16</sup> published one of the first papers to describe a detailed method using radio frequencies despite radio waves being used previously by Mania et al.<sup>16</sup> They used a 1 kW RF generator at 13.56 MHz, along with substrates such as silicon wafers and molybdenum which were heated to 950 °C.<sup>16</sup> The gas mixture employed was a mixture of H<sub>2</sub> and CH<sub>4</sub> with varying CH<sub>4</sub> content from 0.2% to 1%, ensuring low-pressure growth conditions of below 0.03 atm.<sup>16</sup> The gas mixture used was typical for the time. Matsumoto et al.<sup>16</sup> published two separate results, growing films to thicknesses of 5 and 20  $\mu\text{m}$ .<sup>16</sup> However, whilst they did not cite the time allowed for growth and an official growth rate was not published, the rate was most likely fast as growth time would not be more than 10 hours. The rate of growth may not be deemed relevant to the paper, as it is one of the first papers to determine if using RF to form diamond via CVD conditions is possible; nevertheless, the growth rate from this paper would have been of interest.

There are no further studies of significance in terms of the activation method after 1983. However, whilst in more recent papers,<sup>8,9,21,22</sup> microwaves and hot filaments are widely mentioned but research into radio frequencies appears sparse.

## Substrates

The substrate is the surface where deposition of activated carbon species occurs and on which a diamond film will grow. A key property of the substrate is that it must facilitate the nucleation of new carbon upon its surface.<sup>23</sup> Nucleation is a physical process that must happen initially when forming a new crystal, in the case of diamond, from a vapour to a crystalline solid. The first few activated species must form a site to facilitate further deposition, which after time will produce a new diamond film.<sup>23</sup>

A number of early papers<sup>1,11</sup> on synthetic diamond utilised diamond powder as the substrate. Using diamond as a substrate is perfect for deposition due to the powdered diamond surface acting as a nucleation site. However, diamond powder leads to poor film quality due to the number of seeds that can facilitate nucleation, therefore new substrate materials were required to ensure quality. Diamond can also be costly and reducing the cost of a component of the process will make the CVD method a more cost-effective form of growing new diamond.

Due to these reasons, research into non-diamond substrates began in the 1980s. This started with Spitsyn et al.<sup>24</sup> growing diamond crystals on non-diamond substrates such as silicon, copper and tungsten at rates of  $5 \mu\text{m hr}^{-1}$ .<sup>18,25</sup> Furthermore, they noted that spontaneous nucleation occurred on the non-diamond surfaces, especially on the defects of the surface such as scratches.<sup>24</sup> This appeared to be a promising beginning in the research of non-diamond substrates as it showed that more available, non-diamond substrates could be viable options for diamond CVD. This subsequently left diamond powder as an obsolete technique.

In 1982, Matsumoto et al.<sup>18</sup> described a method to grow diamond on silicon wafers and molybdenum plates in a flow system. A flow system is a reactor setup where the gas mixture is passed over the deposition site at a specified flow rate.<sup>18</sup> The material must be able to withstand the reactor conditions and the substrate itself must be heated to over  $700^\circ\text{C}$  whilst the filament heats the chamber to temperatures above  $1000^\circ\text{C}$ .<sup>15</sup> The group also found that both silicon and molybdenum produced diamonds of similar structure. Matsumoto et al.<sup>18</sup> agreed with Spitsyn et al.<sup>24</sup> that diamond growth could be facilitated by non-diamond substrates, negating the need for diamond powders, and moving further toward a standard model for diamond growth.

Silicon wafers are a commonly used substrate,<sup>26</sup> however they may not be the most suitable, depending on the properties of the diamond desired. The substrate must have a similar expansion coefficient to that of the diamond film being produced,<sup>15</sup> this is to ensure the diamond film undergoes the least amount of stress possible as the substrate cools and contracts.<sup>15</sup> Kistenmacher et al.<sup>21</sup> grew diamond film upon a silicon substrate and analysed the experimental results using x-ray crystallography techniques and electron microscopy.<sup>21</sup> They determined that film quality decreases

with thickness, and quality is optimised at thicknesses below 20  $\mu\text{m}$ .<sup>21</sup> From their observations, they concluded that the poor film quality was caused during the growth process rather than the cooling phase, and the defects were determined to be due to the silicon substrate.<sup>21</sup> Therefore, silicon is an unsuitable substrate for diamond growth of high quality films over 20  $\mu\text{m}$ .

### Gas Mixture

In Eversole's 1962 patent, he used a range of gas mixtures within the reactor, including low weight carbon species such as CO, CH<sub>4</sub>, CH<sub>3</sub>Cl and CO<sub>2</sub> along with other molecules such as NH<sub>3</sub> and NO, with CH<sub>4</sub> alone having the largest growth rate of 1.30% weight gain per hour.<sup>1</sup> Literature published in the wake of Eversole's patent were rarely exclusively based upon the gas mixture itself, with papers usually carrying out multiple runs of the same experiment with different gas mixture compositions.

Further key experimental literature was published by Bachmann et al. in 1991<sup>25</sup> and aimed toward a standard gas mixture that would ensure diamond growth. They compiled data from 68 studies producing a diagram depicting the gas mixtures that successfully produce a new diamond film, as seen in Fig. 4. From the C-H-O diagram, it is apparent that diamond growth is restricted to a small area of the diagram<sup>25</sup> showing how sensitive diamond growth is when it comes to the gas mixture.

Whilst there were no experimental results by Bachman et al.<sup>25</sup>, the paper suggested a general idea of what gas mixture may support diamond growth. In addition, it showed gas mixtures that may be interesting to research, such as the hydrogen-free domain, where only carbon and oxygen species are used. Bachmann et al. are referenced prolifically throughout the literature,<sup>9,15,26-28</sup> highlighting the importance of this paper and its content. The authors further concluded that within this domain, controlling the gas temperature was the most important variable to ensure high rates of diamond growth.<sup>25</sup>

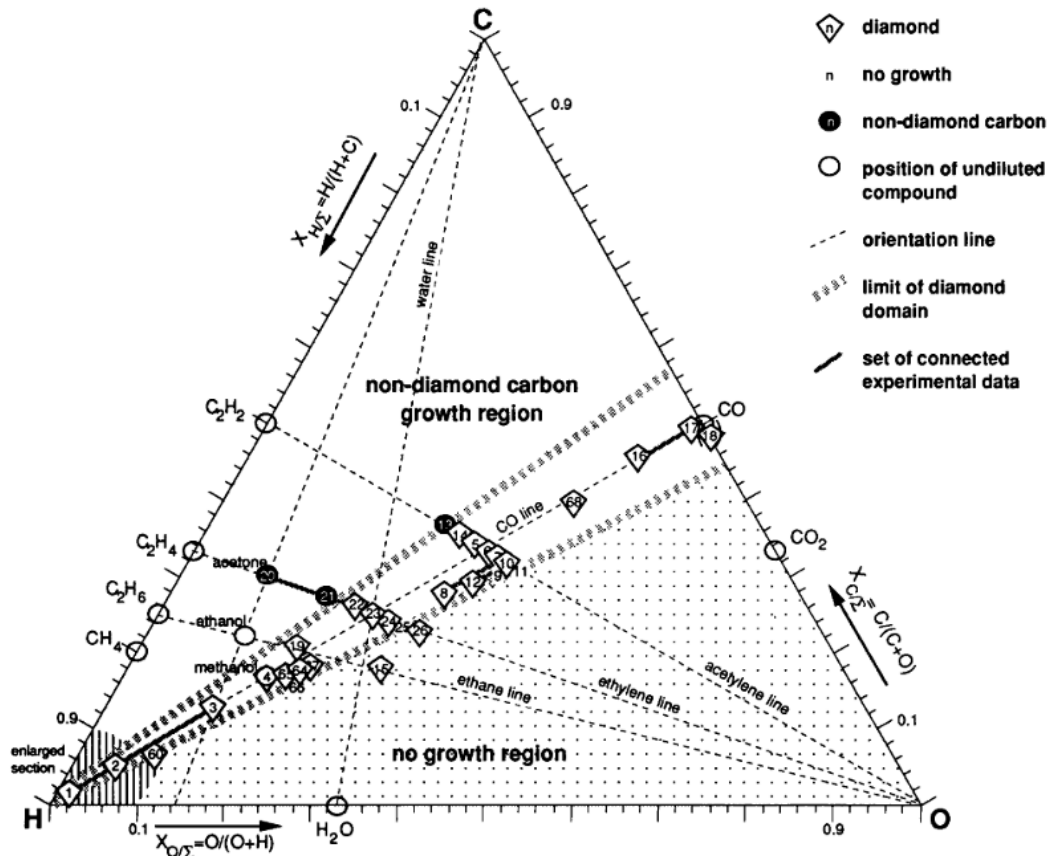


Figure 4 - C-H-O Diagram from Bachmann et al. - Shows the regions of gas composition viable for diamond growth, as well as regions of no growth and graphitic deposition

Whilst not relevant to this thesis, other carbon containing molecules have been researched. Halogen containing species have been included in the hydrogen/hydrocarbon gas mixture, with a proposed purpose of increasing the concentration of atomic H, and in turn increasing the growth rate of the diamond film.<sup>29</sup> Corat et al.<sup>29</sup> explain that while in theory using halogens may benefit the diamond CVD method, halogens are practically difficult to use. The complications halogens cause, for instance the formation of strong acids such as HF and HCl as well as their subsequent corrosion of the reactor may outweigh their benefit.<sup>29</sup>

### Computational Studies

Computational research on diamond CVD commenced after the 1980s. Computational studies attempt to use chemical theory coupled with sophisticated mathematical algorithms to understand the finer details of the growth process, such as energy barrier values and geometry alterations during growth.

The main computational methods in diamond CVD are namely:

- Empirical

- Semi-empirical
- Density Functional Theory (DFT)
- Hybrid functionals

Empirical methods appear outdated when looking at surface energy calculations when compared to today's standard. Authors do still use empirical methods for certain problems where other methods would be too costly. The first computational studies on diamond CVD, employed empirical force-field methods to interpret the mechanism of diamond growth.<sup>30,31</sup>

Semi-empirical methods are a quantum mechanical approach to approximate the Schrödinger Equation, which is done by reducing the number of integrals that are required to produce a Fock matrix, a key step in solving the equation.<sup>32</sup> The most used semi-empirical methods employed are the AM1 and the PM3 models, which have added parameters to reproduce experimental results.<sup>33</sup>

Semiempirical methods are accurate for reactions that have a lot of prior experimental data to input into the functions. Whilst this is a major advantage, it also leads to its disadvantage, as they are unreliable for reactions that have little experimental information.<sup>32</sup> Furthermore, their accuracy and calibration can only be as good as the experimental information collected also. Semiempirical methods are not without their advantages however, as they are able to describe bond breaking and forming processes. However, the main advantage to these methods is that they significantly reduce the computational time, which outweighs its disadvantages.<sup>32</sup>

Density functional theory (DFT) is built upon Kohn-Sham Theory and can be deemed an improvement of Hartree-Fock Theory.<sup>32</sup> The theory was proposed in 1965<sup>34</sup> which suggests a method where the energy of the system is based upon the electron density within the system in question.<sup>32</sup> DFT methods are used prevalently throughout the computational literature,<sup>4,20,35,36</sup> with the method more accurately reproducing experimental results than semiempirical and empirical methods. DFT is not without its limitations, however. DFT's less conventional approach to the Schrödinger equation causes longer computational time when compared to semiempirical methods. This results in DFT functionals being more expensive to utilise.

A further limitation with DFT is that there is no definitive way to improve results without external parameters being applied.<sup>32</sup> Van der Waals is a key interaction that contribute to the overall energy of a system, although unaltered DFT is unable to describe this process.<sup>32</sup> CRYSTAL17,<sup>37</sup> for example, automatically adds a dispersion parameter to all DFT functionals. Whilst these are limitations, computational programmes of today have additional parameters to ensure more accurate calculation of the Schrödinger equation.

Hybrid functional methods are the most recent form of computational calculation cited within diamond CVD investigations and featured prolifically in more recent literature.<sup>4,20,35,38</sup> First devised by Becke<sup>39</sup> in 1993, the method attempts to solve the exchange-correlation energy in terms of Kohn-Sham orbitals, by mixing both DFT and Hartree-Fock methods. A very common functional of this nature is the B3LYP functional, standing for Becke, 3-parameter, Yan-Lee-Parr. This method specifically was first proposed by Becke,<sup>39</sup> using the correlation function from Lee et al.<sup>40</sup> Another prevalent method is the PBE0 functional, first published in 1999 by Adamo and Barone.<sup>41</sup> This functional is a mixture of Perdew-Burke-Ernzerhof (PBE)<sup>42</sup> exchange energy and Hartree-Fock exchange energy in the ratio 3:1. In addition, a correlation energy parameter is added to improve upon the PBE method.<sup>41</sup> Hybrid functionals produce the most accurate results out of all the computational methods mentioned, with the main limitations being the cost. The cost is a consequence of the longer computational runtimes required when using these methods.

Lastly, Monte Carlo models are used quite prevalently throughout computational studies of diamond, especially surface reactions. Monte Carlo (MC) is the general name used for a series of simulation methods for research topics such as equilibrium and dynamic properties of a system.<sup>43</sup> In this review, there are some papers which use the MC model to simulate surface growth<sup>44</sup> along with thermodynamic and kinetic properties of the surface reactions. A kinetic Monte Carlo (kMC) model is produced to mirror the elemental reactions that occur in experimental growth of diamond.<sup>22</sup> Growth species involved in the synthesis of diamond are allowed to attack the surface in random order with the probability of each one reacting with a corresponding surface species.<sup>22</sup> The probability of a reaction occurring is input as a parameter of the simulation,<sup>22</sup> where the parameters of the elementary reactions are the activation energy, and thermodynamics values such as Gibbs free energy, change in heat enthalpy and change in entropy.

In 2015, Rodgers et al.<sup>45</sup> produced a three-dimensional kMC model to simulate deposition upon the (100) diamond surface. The model would simulate the deposition of CH<sub>3</sub>, CH<sub>2</sub>, CH<sub>1</sub>, and C upon the surface, along with the atomic H production being simulated using thermal or electron-impact dissociation. Before this paper, all their previous literature was only using a two-dimensional kMC. Furthermore, the paper simulated the growth of a range of crystal sizes, each one being evaluated and analysed. By using the model to apply a breadth of variable conditions, such as adsorption, etching, nucleation and desorption, Rodgers et al. reproduced the kinetics observed in the diamond CVD growth process.

This paper is mentioned as it successfully showed that the use of a three-dimensional model is possible to reproduce experimental observations convincingly. The model can act as a basis that can be refined

and added to, to simulate diamond growth more accurately in the future, as the paper itself points out its limitations. The model produced a three-dimensional cubic grid which is not completely representative of the real diamond lattice, and not as accurate as the model produced by Netto and Frenklach.<sup>14</sup> The paper states that a compromise was made between accuracy and calculation speed, favouring runtime so more calculations could be carried out.

### Dimer Mechanism

This literature review will focus more on the dimer mechanism of the diamond CVD growth process. There are other mechanistic pathways such as the trough mechanism although it does not apply to this thesis or research, as all computational studies are carried out on the (100) 2x1 reconstructed surface. The reconstruction can be seen in Fig. 5.

The first paper that provided a convincing mechanism was by Garrison et al.<sup>30</sup> This study employed molecular dynamics (MD) simulations to achieve their conclusions.<sup>30</sup> They constructed an eight-layer slab of carbon atoms with the (001) face reconstructed into the (2x1) reconstruction.

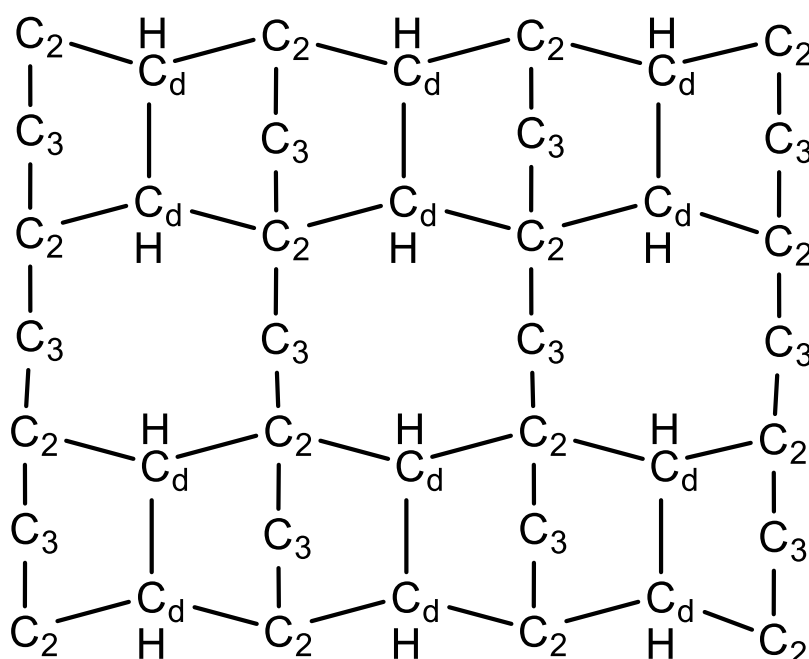


*Figure 5 – (100) - (2x1) Dimer Reconstruction, taken from Skokov et al. (1994), redrawn in ChemDraw*

They then analysed the reactions of the exposed surface by replacing an H with a series of different single carbon moieties such as C, CH, CH<sub>2</sub>, and CH<sub>3</sub>. The energy barrier to methyl adsorption greatly changes throughout the research. If CH<sub>3</sub> is adsorbed to the surface radical, conversion to a CH<sub>2</sub> species via hydrogen abstraction must occur for the growth pathway to continue.<sup>30,31</sup> This is a dominant pathway, as CH<sub>3</sub> is seen as the most abundant activated hydrocarbon species in the reactor.

## Methyl Adsorption at Dimer Sites

From earlier literature,<sup>30,31</sup> external carbon species are required for diamond growth. Therefore methyl adsorption was assumed to occur with rather high probability and is treated as a key step in the simulations due to it being the source of carbon for new film.<sup>46</sup> This warranted research into the surface adsorption reactions.

In 1994, Skokov et al. studied the (100) surface using a hybrid model. A hybrid model is a numerical model where multiple different mathematical approaches are applied to different areas of the simulated structure. In the model, the cluster of central carbons is treated using a PM3 semiempirical method.<sup>3</sup> The neighbouring carbons to the cluster are modelled using empirical methods with the furthest atoms from the reaction zone fixed in position.<sup>3</sup> This may lead to limitations to the method, due to the less accurate empirical method applied to the surrounding atoms. From the simulation, the minimum energy structure of the surface model was found using Hartree-Fock calculations and molecular dynamics also.<sup>3</sup> This taken from Skokov et al.'s previous literature studying growth on the (100) diamond surface.<sup>47,48,49</sup>

From this paper, they concluded that the adsorption of methyl radicals to bridge and dihydride sites always experience energy barriers; this is in contrast with adsorption to the dimer sites.<sup>3</sup>

This is also corroborated by Tamura et al., in 2000, who agree that the CH<sub>3</sub> will readily adsorb with an enthalpy change equal to -351 kJ mol<sup>-1</sup>.<sup>50</sup> Bridge sites are the area that is located between two adsorbed dimer sites of the reconstructed surface, with examples in Fig. 6. Dihydride sites, with examples in Fig. 7, are surface conformers that have two terminated sites with a carbon radical separating them.

A further conclusion from the paper is that methyl adsorption to bridge sites (Fig. 5) is an unviable pathway for diamond growth. Void sites are the empty areas between two adsorbed dimer sites, best depicted in Fig. 6. The group cites potential energy barriers of 2.4 to 24.2 kcal mol<sup>-1</sup> and 7.2 to 29.3 kcal mol<sup>-1</sup> for adsorption to bridge sites and dihydride sites respectively,<sup>3</sup> with the range depending due to the paper analysing multiple conformations of each site. These ranges could be indicative of the inaccuracy of their semiempirical approach and therefore could be a limitation to this study.

From this analysis, they determined that CH<sub>3</sub> adsorption to void sites, seen in Fig. 6, are not a viable way to produce a new diamond film. This is due to the repulsion of the surface H atoms and the incoming CH<sub>3</sub> radical, causing high adsorption energy barriers as well as having a small equilibrium constant, thus having a short lifetime. These reasons result in adsorption of methyl radicals to void sites as an unviable mechanistic pathway for diamond growth and are corroborated by Tamura et al.,<sup>50</sup>

who used the more accurate DFT functionals to collect supporting results. However, they did not calculate the activation energy of these reactions but only the enthalpy changes.<sup>3,50</sup>

In 2008, Cheesman et al.<sup>4</sup> presented evidence that the methyl adsorption to any radical site is a barrierless process, with the an energy change of  $-383.7 \text{ kJ mol}^{-1}$ .<sup>4</sup> This includes the dihydride (Fig. 7) and bridge sites (Fig. 6) quoted in Skokov et al.'s publication and therefore the two conclusions are in complete disagreement.<sup>3,4</sup> Whilst Butler<sup>51</sup> is unsure why there is a difference in the value obtained by the two groups, the computational methods employed in both papers are wildly different.

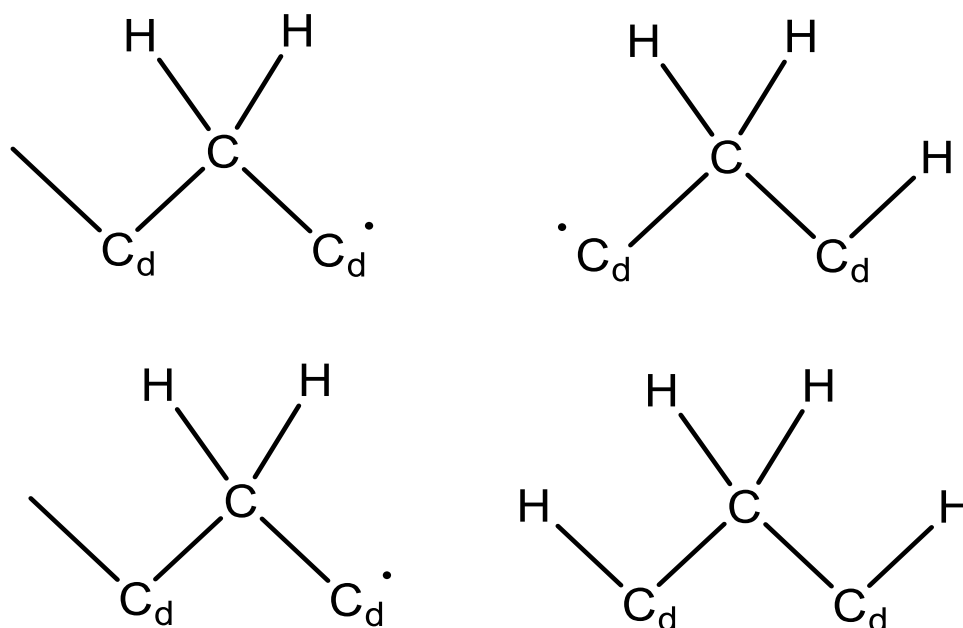


*Figure 6 - Extract from Skokov et al. (1994) depicting examples the Void sites that subjected to methyl adsorption and energetic analysed, redrawn in ChemDraw*

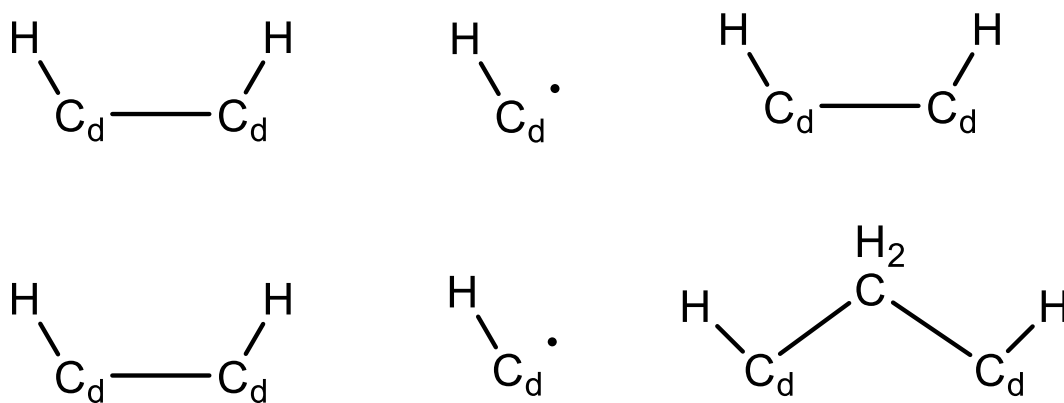


*Figure 7 - Extract from Skokov et al. (1994) - Depicting analysed examples of dihydride sites that were also energetically analysed after simulation methyl adsorption to the radical diamond surface, redrawn in ChemDraw*

The simulation methods used by Skokov et al. means that the model is only accurately treated at short-range distances, as they utilised the semi-empirical PM3 method and less accurate empirical methods on the surrounding atoms. At the time, these methods were believed to be accurate, however, as computational power increased, more sophisticated quantum mechanical methods were introduced, such as the B3LYP hybrid-functional; this is cited in later literature.<sup>4,20,35</sup>

Cheesman et al.'s study used an expensive hybrid functional, B3LYP, coupled with a large, expensive basis set, 6-311G\*\*, to carry out the geometry optimisations of the structures analysed through Quantum Mechanical/Molecular Mechanical (QM/MM) simulations of the surface reactions.<sup>4</sup> The higher degree of sophisticated computational methods is the reason for the difference between the results of these two studies,<sup>3,4</sup> leading to the modern idea that CH<sub>3</sub> adsorption to surface radicals to be barrierless irrelevant of the nature or geometry of the diamond surface radical. To support the accuracy of their model, they calculated the energy barrier to H abstraction from the dimer carbon as 26.4 kJ mol<sup>-1</sup>, which is in good agreement with previous literature by Kang and Musgrave,<sup>20</sup> who used the B3LYP functional also, attaining an abstraction value of 28.5 kJ mol<sup>-1</sup>.

Tamura et al. further investigated the process of adsorption of a CH<sub>3</sub> radical from the vapour to the already adsorbed CH<sub>2</sub>. They explain that this process is both thermodynamically and sterically feasible resulting in steric issues for further growth to occur.

### β-Scission Reaction

Garrison et al.<sup>30</sup> explained that after adsorption of a CH<sub>3</sub> species and its subsequent H abstraction, the dimer bond becomes highly strained which consequently breaks. This forms a double bond with

the adsorbed CH<sub>2</sub>, named a β-scission reaction due to the carbon bond two bonds away from the CH<sub>2</sub> radical being broken.<sup>30,52</sup>

This leaves the adjacent dimer carbon as a radical, which then facilitates the insertion of the CH<sub>2</sub> between the dimer bond and resulted in the addition of an external carbon into the diamond lattice.<sup>30</sup>

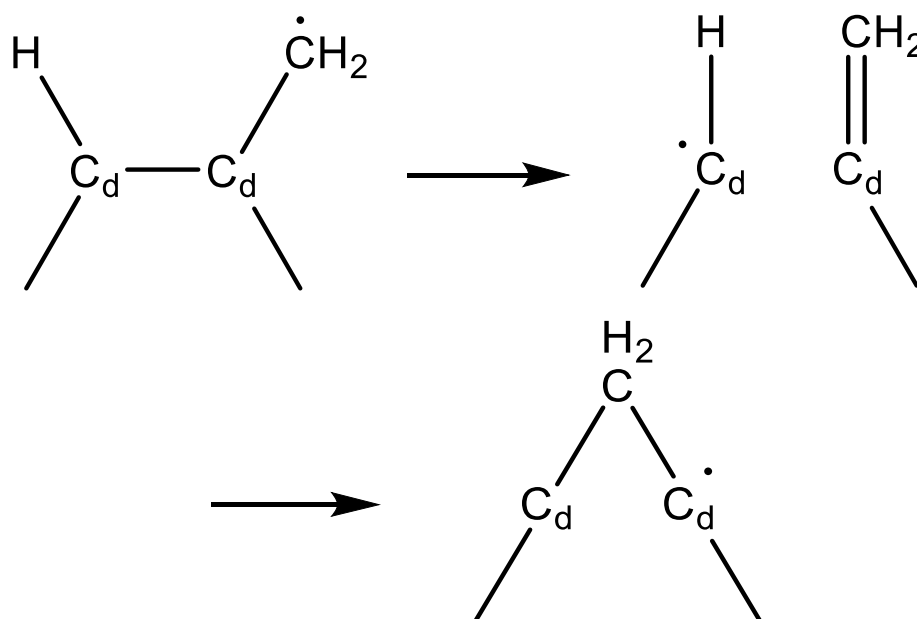


*Figure 8 - Beta-Scission reaction leading to insertion of new carbon onto the diamond's surface, drawn in ChemDraw*

Limitations to Garrison et al.<sup>30</sup>'s study can be due to their use of molecular dynamics to simulate their mechanism. As stated in the paper, many of the structures within the pathway are high in energy due to the presence of radical sites as well as them stating that the β-scission reaction being a high energy reaction also.<sup>30</sup> Molecular dynamics methods only sample the low-energy part of the surface and are not suitable for sampling of high-energy regions,<sup>32</sup> such as the reactions mentioned above. However, the study has been cited by a large number of papers,<sup>4,20,53</sup> and even though the energy values may not be accurate, the number of citations coupled with the lack of challenge, suggest the credibility of its proposed mechanism.

Tamura et al.<sup>50</sup> published the thermodynamic values of this process, which hadn't been done before 2000. They employed GGA (Generalised Gradient Approximation) DFT calculations using a plane-wave basis set, concluding that the insertion of CH<sub>2</sub> is an exothermic process.<sup>50</sup> Furthermore, they explain that the lifetime of the CH<sub>2</sub> is short, due to hydrogen adsorption to the methyl stopping the ability to

carry out the  $\beta$ -scission reaction. Therefore, the  $\beta$ -scission process must happen quickly after adsorption and subsequent H abstraction to ensure growth upon the surface.<sup>50</sup>

The  $\beta$ -scission step is deemed the most important reaction,<sup>53</sup> due to facilitating the insertion of the  $\text{CH}_2$  into the diamond's surface. Both the formation of the double bond to the adsorbed carbon species, as well as the breaking of the dimer bond also, results in this step having a rather high reaction barrier. The barrier to the  $\beta$ -scission is quoted as  $54 \text{ kJ mol}^{-1}$ , found using a variable-step kinetic Monte-Carlo (KMC) model.<sup>53</sup> This is in good agreement with values calculated by Skokov et al. who calculated the  $\beta$ -scission reaction as having an activation energy of  $64 \text{ kJ mol}^{-1}$ .<sup>47</sup> In the same year, Tamura et al.<sup>50</sup> further state that the  $\text{CH}_2$  insertion is also an important process due to it having an energy barrier, quoting values from Kaukonen et al. of  $167 \text{ kcal mol}^{-1}$ .<sup>50</sup>

An issue with this statement is that Tamura et al. appear to treat  $\text{CH}_2$  insertion as one single step, and do not allude to the idea that a double bond is formed after the dimer bond breaks, which seems to be prevalent throughout the literature, before and after the paper's publication in 2000.<sup>31,53,54</sup> This raises the question of whether they were making an accurate approach. This is in contrast with other papers of the time, who deemed the process a crucial part of diamond growth from the dimer mechanism.<sup>53</sup>

### Etching of Adsorbed Carbon Species

In 1999, Battaile et al. used a Monte Carlo Model along with DFT and semiempirical methods to carry out surface calculations regarding etching. They found after analysing prior literature,<sup>3,31</sup> that credible mechanisms were proposed. However, they were not implementing etching kinetics that would affect growth as observed experimentally. Previous models showed results that the (100) surface grew the fastest when compared to the (110) and (111) face. This was a conclusion from Harris and Goodwin<sup>31</sup> in 1993. Experimentally, this is untrue, as the (100) surface grows more slowly than the (110) and is smoother. Battaile et al. believed that the reason for this discrepancy was due to the lack of accurate etching modelling within these simulations.<sup>55</sup>

Etching occurs after the  $\beta$ -scission reaction, where atomic H abstracts a newly inserted  $\text{CH}_2$  from the diamond's surface.<sup>55</sup> Essentially, it is the reverse reaction to the insertion of  $\text{CH}_2$ . Battaile et al. cite the insertion of the  $\text{CH}_2$  as the rate-limiting step due to it being 20 times slower than the  $\beta$ -scission reaction at 1200 K. Harris and Goodwin cited this step to have a very negative Gibbs energy change of  $-88.8 \text{ kJ mol}^{-1}$ , which resulted in their claim that  $\text{CH}_2$  insertion is an irreversible reaction.<sup>31</sup>

However, as stated above, their use of empirical methods such as MM3 caused speculation upon their claims, as molecular mechanics methods are unreliable when treating surface and hydrocarbon

radicals, which are prevalent throughout the topic. This warranted Battaile et al. (as well as another paper<sup>53</sup>) to recalculate these values. Furthermore, Richley et al.<sup>38</sup> present evidence against Harris and Goodwin's claim also, stating that the insertion of CH<sub>2</sub> into the diamond surface from the gas phase would be entropically unfavourable.

Battaile et al. constructed a model of diamond, where around 20 carbons located at the reaction zone, would be treated using DFT methods, although specifically which are not stated.<sup>55</sup> The surrounding carbons to these would be treated using the semiempirical, tight-binding method. Specifically, the semiempirical slab was made up of 5 layers, each with 16 carbon atoms.<sup>55</sup> The model was then simulated using a Monte Carlo model, under conditions typical for a hot filament reactor.

The simulations found that the growth rates were optimal at 1200 K. However, they cite that the experimental observations did not show that a specific temperature was optimal to growth. Furthermore, at a temperature over this value, growth rates decreased. This is due to the CH<sub>3</sub> species desorb more rapidly from the diamond's surface, removing growth species from the diamond. Crucially, Battaile et al. were successful in producing a model that accurately mirrors the growth rates observed experimentally, with simulated etching slowing the growth of the (100) considerably, whilst affecting the growth of the (110) and (111) face much less.<sup>55</sup> Their model also showed that etching facilitates the production of less rough surfaces also, as seen in their simulation diagrams.

In 2005, Netto et al. carried out etching investigations using a Monte Carlo model. They carried out etching upon sp<sup>3</sup> carbons only, with the etching rates ranging from 0 % to 100 %. Whilst etching rates of 25 %, 50 %, and 75 % all showed similar growth rates and surface widths, they found that 0 % etching resulted in no growth at all.<sup>14</sup> This highlights the role of atomic H, as etching ensures that the surface of the diamond is in a state where growth can be facilitated. Without etching, moieties that inhibit growth bind to the diamonds surface, with no species to ensure its removal.<sup>14</sup>

### Undesired Pathways

Tamura et al.<sup>50</sup> simulated the process of adsorption of vapour CH<sub>3</sub> onto the bound CH<sub>2</sub> radical. They determined that this process was both thermodynamically and sterically feasible. In addition, they concluded this process stunted further diamond growth without the later abstraction of the CH<sub>3</sub> or as C<sub>2</sub>H<sub>5</sub>.<sup>50</sup> Growth is halted in this region due to the steric issues caused when forming the new layer. Furthermore, the adsorption of C<sub>2</sub>H<sub>5</sub> is likely, due to the high energy (167 kJ mol<sup>-1</sup>) required for insertion of the CH<sub>2</sub> to occur, as it provides time for the C<sub>2</sub>H<sub>5</sub> species to form in the gaseous phase.<sup>50</sup> In terms of experimental practice, the high concentration of CH<sub>3</sub> in the gas mixture leads to the formation of C<sub>2</sub>H<sub>5</sub> by-product in the reactor before adsorption. Once adsorbed, it stunts diamond growth.<sup>50</sup> Tamura et al. states this fits with the experimental observation that increasing CH<sub>4</sub> to H<sub>2</sub>

ratio decreases crystal quality and ensuring high H<sub>2</sub> content will ensuring the etching of these adsorbed moieties,<sup>50</sup> solving this issue.

### Requirement for Parameter Review

There has been some review of previous literature that published results using MM2 and MM3 semiempirical methods, such as Harris and Goodwin<sup>31</sup> and Skokov et al.<sup>3</sup>. Papers such as Oleinik et al.<sup>53</sup> and Battaile et al.<sup>55</sup> revisited Harris and Goodwin's<sup>31</sup> results in 2000 and 1999 respectively, attempting to understand the problems with their study. Battaile et al. concluded that their MC model failed to mirror experimental results as they did not include etching processes within their model, which resulting in the failure to reproduce experimental results. Oleinik et al.<sup>53</sup> agree with Battaile et al.<sup>55</sup> and made a broader claim that the discrepancies of Harris and Goodwin's<sup>31</sup> paper may have come from missing reaction sets in the model or the inaccurate kinetic parameters for the considered reactions.

Due to this, Oleinik et al.<sup>53</sup> recalculated two key parameters that determine the kinetics of the dimer insertion reaction. These are the activation barrier of the  $\beta$ -scission reaction and the enthalpy of the same reaction. Harris and Goodwin found these values using MM2 and MM3 semiempirical methods whilst Oleinik et al. employed the more accurate tight-binding GGA functionals. These are also a type of semiempirical method, although these are more suitable for high energy species such as radicals compared to MM2 and MM3. They recalculated that the activation energy and enthalpy were 54 kJ mol<sup>-1</sup> and -29 kJ mol<sup>-1</sup> respectively. This in contrast to the previous data of 36.8 kJ mol<sup>-1</sup> and -97.7 kJ mol<sup>-1</sup>. The data presented by Oleinik et al. also was found to agree well with PM3 calculations of the same values by Skokov et al. who found them to be 64 kJ mol<sup>-1</sup> although there is quite a difference in the enthalpy of -61.1 kJ mol<sup>-1</sup> compared to Oleinik et al.'s -29 kJ mol<sup>-1</sup>.

The reliance of accurate external parameters is a major flaw with model simulations and computational chemistry in general, as the model is only ever as accurate as the prior understanding of the underlying chemistry. Furthermore, the kinetic and thermodynamic values that determine the behaviour of the models can be found experimentally, however even these values may not be completely accurate, as Rodgers et al. explain, they found that their kMC model was very sensitive to the Gibbs energy change, which generally is a hard parameter to determine experimentally.

### Relevant Energy Barriers

Kang and Musgrave<sup>20</sup> published computational findings on (100) diamond deposition. This paper provides the activation energy to the H abstraction from the (2x1) dimer surface of a C<sub>37</sub>H<sub>42</sub>, citing 28.4 kJ mol<sup>-1</sup>. Furthermore, they calculated the value of the H abstraction from a gaseous CH<sub>4</sub> to be 37.7 kJ mol<sup>-1</sup>. Using the B3LYP functional along with the 6-311G\*\* basis set, they calculated the H

abstraction value of an ethane molecule to be  $21 \text{ kJ mol}^{-1}$  which is  $12.6 \text{ kJ mol}^{-1}$  lower than the experimentally determined value of  $33.5 \text{ kJ mol}^{-1}$ . Due to this, they extrapolated the data they collected, adding the error to the final energy, which they found to be  $15.9 \text{ kJ mol}^{-1}$ . This resulted an energy barrier value of  $28.4 \text{ kJ mol}^{-1}$ . The extrapolation of their data shows that their model is not accurate without later evaluation to the output values, with external errors needing to be calculated.

Cheesman et al. calculated this value to be  $26.4 \text{ kJ mol}^{-1}$ , agreeing with Kang and Musgrave and used a  $5 \times 9 \times 4$  slab with the same surface reconstruction. Furthermore, the paper employed the 6-31G\* basis set for the geometry optimisations, and the 6-311G\*\* for the energy calculations. Therefore, whilst a smaller basis set was used for the geometry optimisations, the model constructed is almost five times larger than that constructed in Kang and Musgrave's study, producing more accurate results.

## Summary

To summarise, diamond CVD is a constantly improving field of research, with a key goal of synthesising diamond more efficiently with specific features that are better suited for application. The conception of the low pressure method began in 1962, with interest in the topic only growing despite corporations turning their attention towards high pressure methods.<sup>27</sup> Major progress in the method's refinement was made throughout the 1980s, with major contributions from research groups such as NIRIM.<sup>16-18,56</sup> This was in addition with attempts towards a standard gas mixture at the end of the decade.<sup>25</sup>

At the start of the 1990s, computational methods became sophisticated enough for quantum mechanical and Monte Carlo simulations to be carried out on large systems such as diamond. This led to the better understanding and agreement of the mechanisms that produce new diamond. This does not imply that experimental studies did not continue, with studies into the use of halogens<sup>29</sup> and inclusion of oxygen<sup>57</sup> into the gas mixture.

By the end of the 1990s and the start of the new millenium, cogent approximations of reaction energy barriers were made, permitted by the introduction of hybrid functionals, which solved the Schrödinger equation more accurately than previous methods. Furthermore, the use of Monte Carlo simulations solved discrepancies between computational and experimental observations of growth rates of the (100), (110) and (111) faces.

More recently, a three-dimensional Monte Carlo<sup>45</sup> model has been introduced and more efficiently described processes which lead to diamond growth as well as whole mechanisms being energetically mapped by Cheesman et al. in 2008.<sup>4</sup> However, there is a clear limitation to computational calculations, as they are usually only as accurate as the input parameters from previous literature.

Papers such as Harris and Goodwin<sup>31</sup> are an example of this, where etching reactions were not included and poor results were produced. Furthermore, many of these models are sensitive to parameters such as Gibbs energy,<sup>45</sup> which is cited as being experimentally difficult to accurately determine. Issues such as these are solved, but usually years later and thanks to new, more sophisticated, computational methods. From this, it can be implied that the understanding of the underlying chemistry in diamond CVD will only become greater as long as computational methods keep improving and the interest in the field persists.

## Aims of the Thesis

The thesis used periodic boundary density functional theory (DFT) to attempt to calculate the energy barriers of hydrogen adsorption and abstraction to and from the (100)-2x1 reconstructed dimer carbon. The model was constructed in the CRYSTAL17<sup>37</sup> programme and was treated with DFT methods whilst the tolerance parameters used are noted. The geometries of the calculated structures were then investigated.

The periodic model tries to replicate the interactions experienced on the reconstructed diamond surface with the periodic construction of the system. This implies both long and short distance interactions are accounted for and this, in turn, will produce closer energy barrier values to that of literature, ensuring a better representation of the bulk surface simulated. The calculations carried out in this thesis exclusively use the 6-31G basis set, a reasonably small basis set that will reduce computational runtime and therefore cost. Investigations into the accuracy of this basis set and the 6-31Gpd basis set are conducted using PBE and the hybrid functionals such as the PBE0 and B3LYP.

The cost of calculation was recorded and analysed during the research, with a key goal of the thesis to see how closely the literature can be estimated using smaller basis sets and cheaper functionals such as PBE. This is a less accurate computational method so the transition state (TS) energy, as well as initial and final structure energies, are deemed as approximations. After the energies were calculated and evaluated, more expensive computational methods were implemented, specifically the B3LYP hybrid functionals. From the difference in results, a very brief cost-benefit analysis was undertaken to demonstrate if hybrid functionals are beneficial compared to extrapolating DFT data, such as the results presented in Kang and Musgrave.<sup>20</sup> The analysis will be achieved by observing the time required for the calculations to converge as well as the overall runtime of systems.

A further aim of the research was to determine the effects of applying polarisation to the lattice on the H abstraction and adsorption barrier. Specifically, the thesis looks at the effects that polarisation has on each additional layer as well as the impact the interaction has on the computational run time. Polarisation has been applied in terms of layers, with an unpolarised system investigated also. From the data produced, conclusions on the necessity of applying polarisation to the system shall be made.

## Methodology

### Basis Set Investigation

The lattice parameters calculated by the following basis sets were investigated: STO-3G, 3-21G, 4-21Gpd, 6-21Gpd, 6-31G, 6-311G and the 6-31Gpd basis set. There were two aims concerning these basis sets. The first, was which one was most suitable for the energy barrier calculations; the second was to obtain the lattice parameter calculated by each set. This would help determine which was most suitable and would produce the necessary lattice parameters required for the input files. Whilst most of the results from this are not significant, the exercise provided practise using the programmes that would be implemented in the core of the thesis. In addition, the investigation would help to determine which basis set would be used in the barrier calculations. The results of the investigation, seen in Table 1 and 2, led to the use of the 6-31G basis set, which was applied to the necessary input files to estimate the H adsorption and H abstraction energy barriers.

Furthermore, investigations into how the lattice parameter differed when varying functionals were applied to the crystal were undertaken. The lattice parameters were recorded for the PBE and B3LYP functionals and displayed in Tables 1 and 2.

It should be noted that in this section, no external polarisation has been applied to the systems, and the results have been obtained solely using the necessary basis sets and functionals.

### Tolerances

CRYSTAL17 employs the self-consistent field (SCF) method to solve the Schrödinger Equation (SE). This approximates the Hamiltonian factor to solve the equation and produce an estimation of the orbitals.<sup>32</sup> The orbitals are subsequently solved again, until the value converges to a more accurate description.<sup>58</sup> Ensuring appropriate tolerance parameters, in turn, ensures the convergence of the SCF. However, the need for larger tolerances results in greater run costs, as the complexity of calculation increases.

The tolerances considered during the calculations were parameters such as TOLINTEG, TOLDEE and SHRINK. Default tolerance values were implemented initially with each parameter being altered or increased if the calculation failed. Taking this approach ensured that run time was minimised and in turn cost of calculation.

TOLDEE is a parameter that governs the convergence threshold on the energy of the system being investigated.<sup>37</sup> The input value used for this parameter is the integer exponent, describing the value at which the calculation should stop converging i.e.  $10^{-\text{value}}$ . This value was kept at 8 as the calculations were running smoothly at this value and no issues at this parameter were found.

SHRINK is a parameter that determines the number of k points created in reciprocal space which are then used in the calculation.<sup>37</sup> Less k points were required when a larger basis set is utilised or if a more complex functional is employed such as B3LYP. Although, as the 6-31G basis set was used exclusively in the barrier calculations, the SHRINK factor was not changed due to the basis set. This parameter was kept at 6 6 throughout the basis set investigation. In the barrier calculations, the SHRINK factor was left at a less expensive parameter of 2 2 for the PBE functional. Although for the B3LYP functional, SHRINK was increased to 6 6 to encourage convergence of the SCF.

The TOLINTEG parameter ensures the accuracy of the calculation of the Coulomb and HF exchange energies.<sup>37</sup> The tolerance acts as a cut off that discards integrals that are produced from overlap of orbitals less than the input value. This slightly reduces accuracy but reduces computational runtime also.<sup>37</sup>

TOLINTEG was the only parameter that was modified during the basis set investigation. The larger basis sets and more sophisticated functionals required a greater degree of tolerance. The 6-31G basis set required 6 6 6 6 12 for all three functionals investigated (PBE, PBE0 and B3LYP) although for the 6-31Gpd basis set required an input tolerance of 7 7 7 7 14 for both the PBE0 and B3LYP functionals. Concerning the energy barrier values, TOLINTEG was kept at 6 6 6 6 12 for the DFT and B3LYP calculations. The cheaper tolerance was used for the calculation of the terminated and radical systems as well as the determination of the TS.

## Functionals

The simplest of the functionals that was used to investigate the lattice parameters and energy barriers was the PBE functional. PBE is a GGA type functional that is composed of an exchange energy term as well as a correlation term. The method was published in 1996 by Perdew et al.<sup>42</sup> who, in the wake of Becke et al.'s B3LYP functional,<sup>39</sup> aspired to search for a simpler method to find the exchange energy term that can be applied to the popular hybrid functionals.<sup>42</sup> In this thesis, a parameterised version of this functional was used, PBE-D3, which ensures dispersion interactions are accounted for also.<sup>37</sup>

PBE0 is a hybrid functional produced by Adamo and Barone in 1998, combining ratios of the PBE functional and HF theory in 3:1 ratio.<sup>41</sup> B3LYP is probably one of the most widely used hybrid functionals within the literature, quoted in a range of papers.<sup>20,35,38</sup> Both of these hybrid functionals will have some parameter investigations done, to decide which should be used to obtain the more accurate energy barrier values.

## Layers Determination

The number of layers employed into the model was found through calculations, evaluating the energy of each system as well as the CPU runtime of each calculation. After looking at these values, seven layers of carbon atoms would be inserted into the model to simulate the H adsorption reaction. A 7-layer structure was deemed a sensible compromise between run-time and ensuring that the top and bottom layers of the lattice would be non-interactive.

## Model Construction

All structures were constructed in CRYSTAL17, with the (100) - (2x1) reconstruction formed first. This was done by producing a conventional diamond unit cell and cutting it in the z-axis to produce a slab. Reconstruction of the surface was then carried out and the surface was terminated with hydrogen atoms. The reconstruction was formed on both the top and bottom layers of the structure, with both being terminated by H also. This was due to the model applying periodic boundary conditions in the x and y directions but not in the z-axis, therefore coding the bottom layer to be terminated was required. This ensured the programme would not take energy calculations of a lattice that has a layer of carbon radicals. The seven layers implemented into the lattice further ensured bulk characteristics of the diamond, producing shielding between the top and bottom layers, ensuring the two layers are totally non-reactive. Lastly, when constructing the unpolarised system, the lattice parameter calculated by the corresponding basis set and functional, needed to be inserted into the input file. The inserted lattice parameters can be seen in Tables 1 and 2.

## Polarisation Application

The next step was to apply the polarisation to the necessary atoms. An unpolarised system, along with systems with one, two and three carbon layers of polarisation were investigated in this thesis. To apply polarisation the necessary atoms, the ATOMSUBS command was used, followed by the number of atoms being polarised. The index of each atom followed this along with 106 or 101, which denoted whether the atom is a carbon or a hydrogen atom.

It should be noted that each layer of the crystal in the unit cell contains eight carbon atoms. In all cases of polarisation being applied, the top layer of H atoms also had polarisation applied. Therefore, the unpolarised, one-layer, two-layer and three-layer systems have 0, 16, 24 and 32 atoms have polarisation applied respectively. The final energy of each system was recorded and applied to Equation 1.

## Formation of the Surface Radical

After each structure was produced, a dimer hydrogen atom was removed, forming a carbon radical. (In this thesis, the structure containing the surface carbon radical will be referred to as the c-radical structure.) This was carried out using the ATOMREMO command, where the number of atoms being removed (one) is stated, along with the index of the atom in question. As a radical is formed, electron spin must be applied to the new c-radical to ensure the energy of the system is accurate. To do this, ATOMSPIN was inserted into the input file, with the carbon atom having +1 spin applied.

FRAGMENT is a command that is required as it relaxes the desired atoms, ensuring more accurate values. The top five carbon layers and the top H atoms were all input into the FRAGMENT block, and relaxed. This was applied to both the c-radical structures and the hydrogen scan structures also. Furthermore, as only the closest H in the H<sub>2</sub> was being scanned, the other H must be included in the FRAGMENT block in order to ensure it is relaxed with the scanning H. Otherwise, it would simply unbind and remain in its starting position, leading to inaccurate energy values. The final energy of each carbon radical system was recorded and used in Equation 2.

## Hydrogen Scanning

An H<sub>2</sub> was inserted above and was scanned towards its final position in increments of x angstroms towards the c-radical, directly to the identical position the H had been removed from when forming the radical. At each scan, the programme relaxes the structure. The molecule was inserted approximately 1.5 Å above its final position using the ATOMINSE command. This distance was a compromise between the computational runtime and ensuring a defined energy curve. The final coordinates were taken from the fort.34 geometry file of the terminated system to ensure the accuracy of its final position.

The energy of the system was calculated by the programme at each scan towards the final coordinates, which were compiled and then evaluated. By running scans with the H<sub>2</sub> molecule bond length set to the literature value of 1.0 Å it was found that the H-H bond immediately broke once scanning began, leaving an H atom above the diamond lattice. A bond length of 0.8 Å was found to solve this issue and was consequently applied to all scans.

Whilst plotting and comparing the adsorption curves of each system may be interesting, the main goal of this was to find the energy at the peak of the curve. This energy is required in both Eq. 1 and 2, to calculate the energy barriers of both the hydrogen adsorption and abstraction energy barriers.

## Energy Barrier Calculations

The energy barrier values are the main results being collected in this thesis. Simple TS theory is used to find the values of the energy barriers required. The energy values required to find the energy barriers of the H adsorption and H abstraction from the diamond reconstruction can be found in Equations 1 and 2. The TS energy is found at the peak of the hydrogen scan curves. The other required energies are produced using the CRYSTAL17 and are collected using a command on the necessary output files, producing the energy of each system.

The energy barrier to the H abstraction process is found using the formula:

$$E_{abstraction} = E_{TS} - (E_{terminated} + E_H)$$

*Equation 1*

Where  $E_{TS}$  is the energy of the transition state,  $E_{terminated}$  is the energy of the fully hydrogen terminated (100) diamond reconstruction and  $E_H$  is the energy of the isolated atomic H.

The energy barrier to the H adsorption process is found using the formula:

$$E_{adsorption} = E_{TS} - (E_{c-radical} + E_{H_2})$$

*Equation 2*

Where  $E_{c-radical}$  is the energy of the diamond reconstructed system that has a single surface radical.  $E_{H_2}$  is the energy of the isolated hydrogen molecule.

Calculating the TS is the most accurate way of calculating the energy barrier with separate files. Another approach towards this would be to use both the energies of the initial and final structures from the hydrogen scan curve. To do this, the first and last points of the curve would be combined with the TS energy to find both barriers. This approach was considered but was decided against as the energies of both structures may be inaccurate, caused by interactions between the hydrogen moieties and the diamond surface.

## B3LYP Calculations

To calculate the B3LYP values, single-point energies of each system (terminated, radical and transition state) and the total CPU runtime were recorded. By removing the OPTGEOM block, this would negate the optimisation of the systems geometry. This approach would produce less accurate approximations although will save a vast amount of time as the geometry optimisations do not take place. This was done after the PBE-D3 calculations were carried out by copying the necessary fort.34 files into the

correct directories. Therefore, the energy of the systems that have been geometrically optimised using the PBE-D3 functional are now being calculated using B3LYP. All the single-point calculations were carried out using 6-31G/B3LYP and calculated using four nodes. Regarding the TS, the spin to the bonding dimer carbon must be removed as it is now partially bonded to the incoming H.

### Computational Runtime

The computational run time is a critical parameter that will allow for several conclusions to be made. Firstly, it will highlight the economic implications of applying polarisation and the degree of polarisation that is appropriate for less expensive research into reactions on the reconstructed diamond surface. Furthermore, the difference in the cost of using the PBE-D3 and B3LYP functionals were compared using the time both the functionals required for the SCF to converge. The time was found in the TELAPSE section of the output file. This approach was a minor compromise, due to the issues experienced with the optimisation of the B3LYP functional. This will be expanded upon within the limitations section of the thesis.

### Geometry Observations

Geometry measurements of the terminated, radical and TS structures have been compiled and discussed. All the measurements were taken from the output file and geometries of structures calculated using the PBE-D3 and B3LYP functionals were both investigated. CRYSTAL17 carries out geometry optimisations to find the lowest energy structure after the SCF has converged. These optimisations should differ depending on the polarisation being applied. The dimer bond, in addition to the interlayer bond length, has been recorded for all varying polarisations. The interlayer bond length is exclusively the bond length between the dimer carbon and the bonded carbons in the second layer of the system. Both the interlayer bond lengths of the terminated and radical systems have been recorded. Taking observations of each system's geometry is necessary to see how applying different degrees of polarisation affects the diamond structure. From these results, conclusions on whether applying polarisation using CRYSTAL17 is appropriate in order to obtain accurate results.

## Results and Discussion

### Lattice Parameter and Basis Set Calculations

Whilst a range of basis sets were investigated, accurate results to the literature were produced from the 6-31G and 6-31Gpd basis sets. The results from these two basis sets were compiled as they influenced the decision on which basis set to employ to the energy barrier calculations. Varied functionals were also applied to both basis sets, including PBE, PBE0 as well as B3LYP. The values collected can be seen in Tables 1 and 2.

**Table 1 - 6-31G Basis Set Calculations Including Functional Variations. Shows Band Gaps, Lattice Parameters, Energy of the system and the runtime required to produce the data.**

6-31G			
	PBE	PBE0	B3LYP
Band Gap, eV	4.2127	6.0705	5.9184
Lattice Parameter	3.601	-	3.604
Energy, AU	-304.495	-304.532	-304.631
Runtime, s	663.424	13257.1	10276.32

**Table 2 - 6-31Gpd Basis Set Calculations Including Functional Variations. Shows Band Gaps, Lattice Parameters, Energy of the system and the runtime required to produce the data. The lattice parameter of the hybrid functionals could not be obtained.**

6-31Gpd			
	PBE	PBE0	B3LYP
Band Gap, eV	4.0834	5.9565	5.8378
Lattice Parameter	3.588	-	-
Energy, AU	-304.562	-304.609	-304.708
Runtime, s	1404.4425	25439.9345	19048.6955

Tables 1 and 2 show data that agrees with existing theory, that the more complex basis set will produce more accurate results. Although, the increase in complexity does warrant more computational time. Firstly, the 6-31G and 6-31Gpd basis sets are equivalent in gaussian functionals although for the 6-31Gpd set applies polarisation to the heavier atoms, such as carbon. This results in greater time for CPU runtime for each set of functionals, which is seen when comparing Tables 1 and 2.

The literature value for the band gap of diamond was cited in 2010 as 5.47 eV.<sup>26</sup> The accuracy of these functionals can be seen in the percentage error in the band gap. The 6-31Gpd/B3LYP and 6-31Gpd/PBE0 shows a 6.6% error and an 8.9% error respectively, whereas the 6-31G/PBE0 and 6-31G/B3LYP express errors of 9.7% and 8.2% respectively. This corroborates the claim that the extra polarisation to the system increases accuracy. However, it also increases runtime considerably, for example, the increase in runtime between the 6-31G/B3LYP to 6-31Gpd/B3LYP increases by almost

86% between change in the basis set. Whilst the more complex basis set produced more accurate values, the aim of this thesis and the considerable increase in computational runtime were both considered when deciding the necessary basis set for the energy barrier calculations. Whilst only the SHRINK input of 6 6 was used, increasing the number of k points would increase the accuracy of the hybrid functionals.

The published runtimes above also show the theoretical trend concerning the functionals, with the less complex 6-31G/PBE and 6-31Gpd/PBE taking a total of 11.1 and 23.4 minutes per node respectively. In contrast, the hybrid functionals (PBE0 and B3LYP) took considerably longer to calculate due to their nature of mixing different computational methods. The 6-31G/B3LYP and 6-31Gpd/B3LYP required 2.85 and 5.29 hours per node respectively. The PBE0 functional required the most amount of computational power though, with 6-31G/PBE0 and 6-31Gpd/PBE0 using 3.68 and 7.07 hours per node respectively.

Overall, this shows that the hybrid functionals are far more expensive, whilst a more accurate way to computationally analyse large systems such as a terminated diamond lattice. They are more accurate as they geometrically recreate the diamond lattice more closely to the literature. The percentage increase from the DFT PBE method to the hybrid functionals was a runtime increase between 1200 (B3LYP) to 1900% (PBE0) depending on the hybrid functional used. This reinforces the need cheaper methods to calculate large systems such as diamond. The DFT approximations can act as a base for further computational research, rather than using the most expensive method immediately. In addition, due to the large runtime increase from PBE to PBE0 compared to PBE to B3LYP, B3LYP was deemed a more suitable functional for the core of the thesis investigation.

Lastly, an investigation into the change of the lattice parameter was carried out. The experimental lattice parameter for diamond is cited as 3.5664 Å.<sup>24</sup> The 6-31G basis set produces a rather accurate approximation of the lattice parameter, even with the cheaper DFT methods such as PBE. 6-31G/PBE produces a lattice parameter of 3.603 Å, which has a percentage error of only 1.03 % to that of the literature. In addition, the 6-31Gpd/PBE produces an even more accurate approximation of 3.588, resulting in a percentage error of 0.61 %. Interestingly, the 6-31G/B3LYP produced a less accurate value of 3.604 Å. This meant that a different value needed to be applied to the model construction that had B3LYP applied.

These values imply that the B3LYP calculates the unit cell to be marginally larger than the unit cell calculated by the PBE functional, which is less accurate. Therefore, the geometry of the crystal may be slightly expanded compared to the literature value and the PBE calculated systems. The deviation in this parameter will be mentioned in the geometry section of this thesis.

## Terminated and Radical Energy Data

Observations can be made from the data presented in Tables 3 and 4 as well as in Fig. 9, that show consistency in the programme's calculations. Firstly, the energy of the system decreases as the degree of polarisation increases in almost all instances, fitting the theory that added polarisation allows for lower energy geometries. However, there is a huge difference between the calculation of the energy of the terminated, unpolarised system. The B3LYP functional calculates the unpolarised, terminated system at a far lower than the other B3LYP calculated terminated systems, producing an energy value that does not fit the trend seen by the other degrees of polarisation.

**Table 3 - Energy Change in the terminated and radical systems as the degree of polarisation is increased. Both the PBE-D3 and B3LYP functionals are used to calculate the final energies of these structures.**

Terminated and Radical Systems					
Degree of Polarisation	Number of Atoms Polarised	Terminated System Energy, AU		C-Radical System Energy, AU	
		PBE-D3	B3LYP	PBE-D3	B3LYP
Unpolarised	0	-2140.84	-2142.05	-2140.18	-2140.87
One Layer	16	-2141.00	-2141.62	-2140.33	-2140.96
Two Layers	24	-2141.14	-2141.70	-2140.47	-2141.04
Three Layers	32	-2141.28	-2141.78	-2140.61	-2141.11

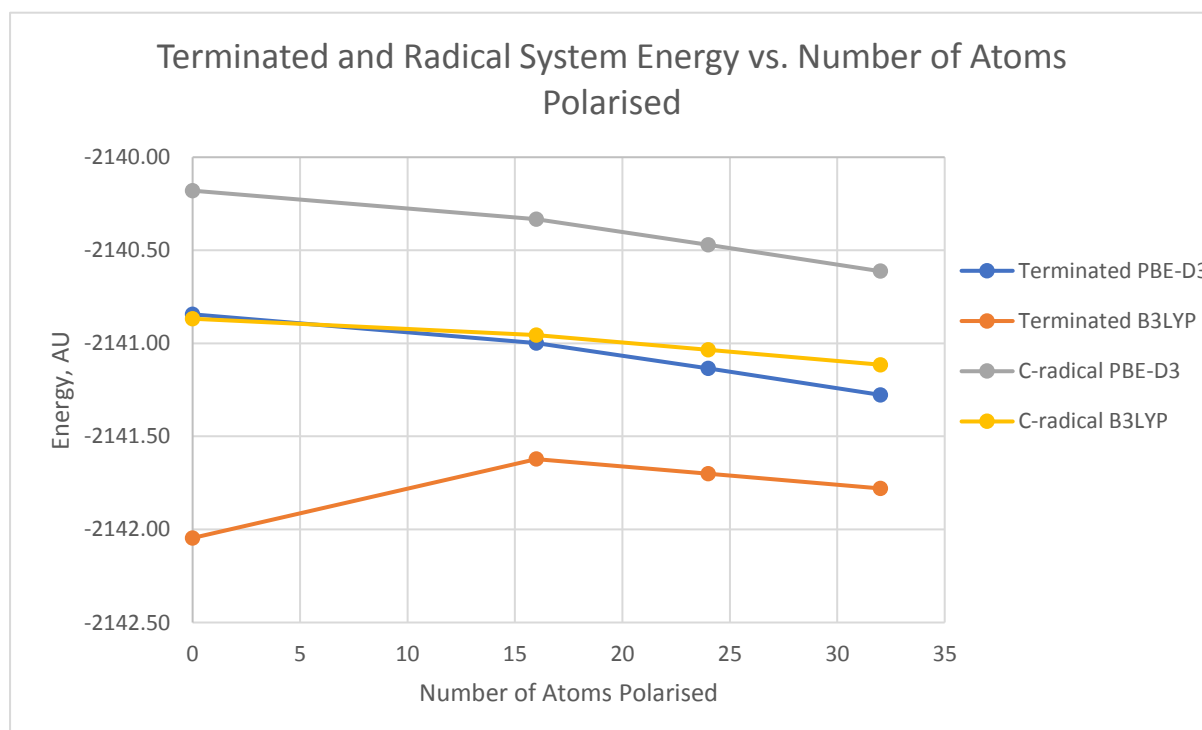


**Figure 9- Figure produced using the data in Tables 3 and 4. It shows all four sets of data, producing comparable curves. TOLINTEG: 6 6 6 6 12, SHRINK: 2 2, TOLDEE: 8**

Despite this anomaly, both the B3LYP and PBE-D3 functionals produce data that corroborate each other and support the claim that applying more polarisation to a system, decreases its energy. This could infer that B3LYP functionals are unsuitable for calculations of unpolarised systems. However, the B3LYP functional does seem to calculate the energy of the unpolarised radical structure that fits with the produced trend.

**Table 4 - Difference in energy between the radical and terminated diamond reconstructions, calculated using the data from Table 3.**

Degree of Polarisation	Number of Atoms Polarised	Energy Difference Between Radical and Terminated Systems, AU	
		PBE	B3LYP
Unpolarised	0	0.66	1.18
One Layer	16	0.67	0.67
Two Layers	24	0.66	0.67
Three Layers	32	0.66	0.66

Using the data from Table 4, the difference in energy of the terminated and radical diamond systems can then be calculated. Negating the B3LYP unpolarised system, this difference between the two systems are very similar, with an average difference of 0.664 AU. Not only does the data in Table 4 support the claim that the programme is consistent, but this data may have provided a less expensive way to approximate the energy of a c-radical system for future studies.

Rather than producing the radical input file and calculating the energy, the terminated system could be calculated, and a value of 0.664 AU could be added to the final, optimised energy. This would reduce the CPU runtime considerably, as the need to construct and calculate the SCF for the radical system would be removed. From the data in both Table 4 and Table 8, the computational runtime that could be saved by undertaking this method ranges from 31.72 to 92.53 hours per node. This is a considerable amount of time that could be negated by executing the presented approximation method.

## Hydrogen Scan Data

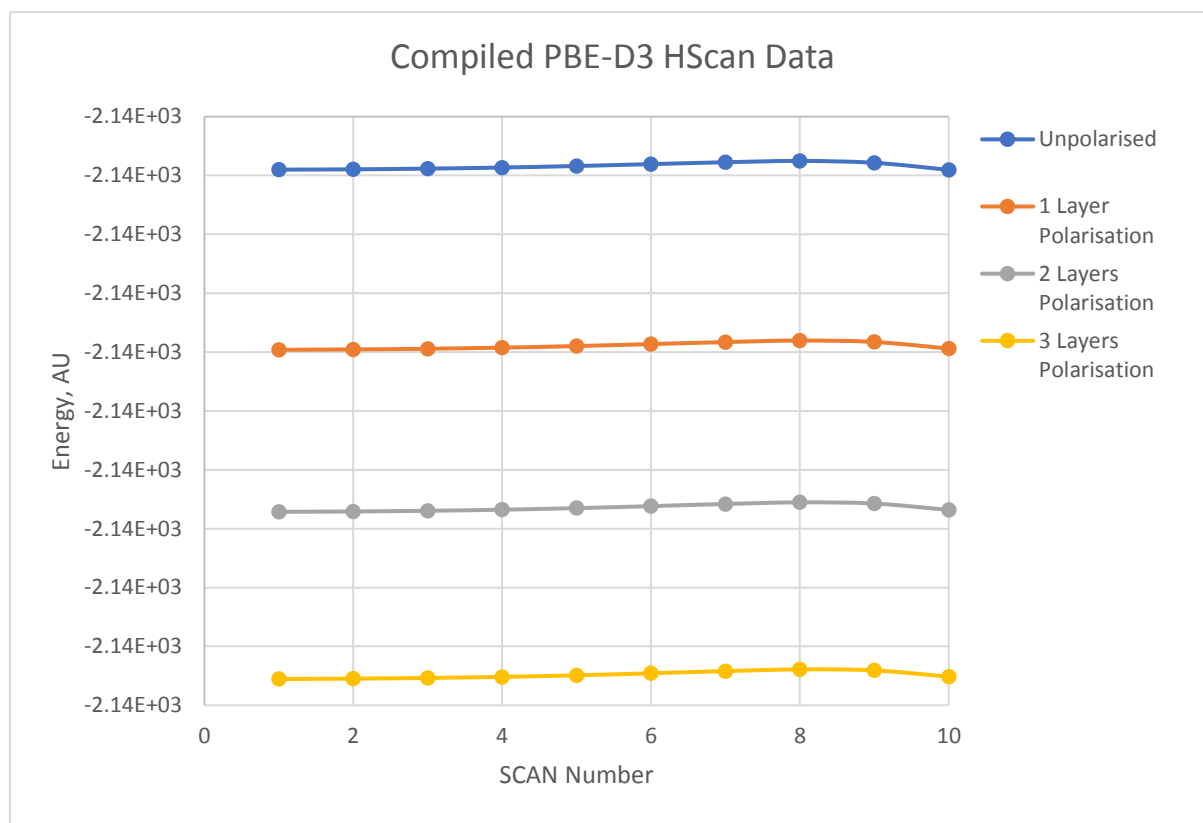


**Figure 10 - Hydrogen Scan Energy Data – Each curve shows the energy of the system as a hydrogen molecule approaches a diamond surface dimer radical. The blue is the unpolarised system. The orange is the system with one-layer of polarisation. The grey is the system with two layers of polarisation applied. The yellow is the system with three-layers of polarisation applied. TOLINTEG: 6 6 6 12, SHRINK: 2 2, TOLDEE: 8**

From the data in Fig. 10, the programme correctly applies polarisation to the adsorption reaction. Polarisation facilitates more orbital interactions, lowering the energy of the lattice structure and therefore the TS of the adsorption/abstraction reaction. This is observed in the consecutive reduction in energy as more layers of polarisation are applied. This data corroborates the data shown in the in Fig. 9 and the claims made in that section. The values of the transition states are seen at the peaks (SCAN 8) of each of the curves, which are better depicted in Fig. 10. The increasing number of layers that are polarised allows for greater flexibility in the diamond system. The greater flexibility in the lattice means the geometry can be optimised to a less energetic geometry, including the transition state of the adsorption/abstraction reaction also.

As polarisation is consecutively applied, it can be seen from Fig. 10 that the difference between the unpolarised and one-layer curves is slightly larger than the difference between the systems. The difference in  $E_{TS}$  of the unpolarised and one-layer system ( $E_{0 \rightarrow 1}$ ) is 0.1526 AU. The difference between  $E_{TS}$  of the one-layer and two-layer system ( $E_{1 \rightarrow 2}$ ) as well as the two-layer and three-layer system ( $E_{2 \rightarrow 3}$ )

is 0.1374 AU and 0.1419 AU respectively, showing a more similar change when further polarisation is applied. This can be explained as the one-layer system has the top layer of hydrogen atoms as well as the top layer of carbon atoms polarised. This differs from the unpolarised system where no atoms are polarised.

Using this data and Eq. 3, the reduction in the TS energy due to the polarisation of only the top layer of hydrogen atoms, can be approximated. From Eq. 3, polarising only the hydrogen atoms will reduce the TS energy by 0.0129 AU. This implies that the polarisation of seven hydrogen atoms reduces the  $E_{TS}$  by a value which is only 9.23 % of the reduction caused by polarising 8 carbons.

$$\Delta E_{Hpolarisation} = E_{0 \rightarrow 1} - \frac{(E_{1 \rightarrow 2} + E_{2 \rightarrow 3})}{2}$$

*Equation 3*

Eq. 3 shows the energy change in the TS if only the surface layer of hydrogen atoms is polarised. Where  $E_{0 \rightarrow 1}$  is the difference between the TS energy of the unpolarised and one-layer system.  $E_{1 \rightarrow 2}$  is the TS energy difference between the one-layer and two-layer systems and  $E_{2 \rightarrow 3}$  is the difference between the TS energy of the two-layer and three-layer systems.

Whilst these are only observations, this could lead to a further reduction in the computational cost to calculate large systems such as diamond reconstructions. The polarisation of seven hydrogens and eight carbons leads to the requirement of around 36 hours per node extra to calculate their corresponding hydrogen scan curves, which are seen in Table 7. However, further investigations into the effects polarising different types of atoms would be required in order to make a strong conclusion.

Furthermore, the shapes of the curves that are produced are nearly identical. This is an interesting observation, as it shows that applying polarisation decreases the energy of the terminated and radical system, whilst showing consistency in the curve. In conjunction, the  $E_{TS}$  is always located at SCAN 8 for all polarisations. For example, the similarity between the energy curves for the unpolarised and three-layer system can be seen in Fig. 11. This further supports that the programme is consistent in its calculations (ensuring the correct parameters are inserted). Furthermore, this is a consequence of the correct coordinates being inserted, such as the  $H_2$  starting coordinates as well as the final coordinates applied to the terminating H of the  $H_2$ . The starting  $H_2$  z-axis coordinates were the same throughout all the scans. This produced a more comparable set of data, controlling variables that were not being investigated.

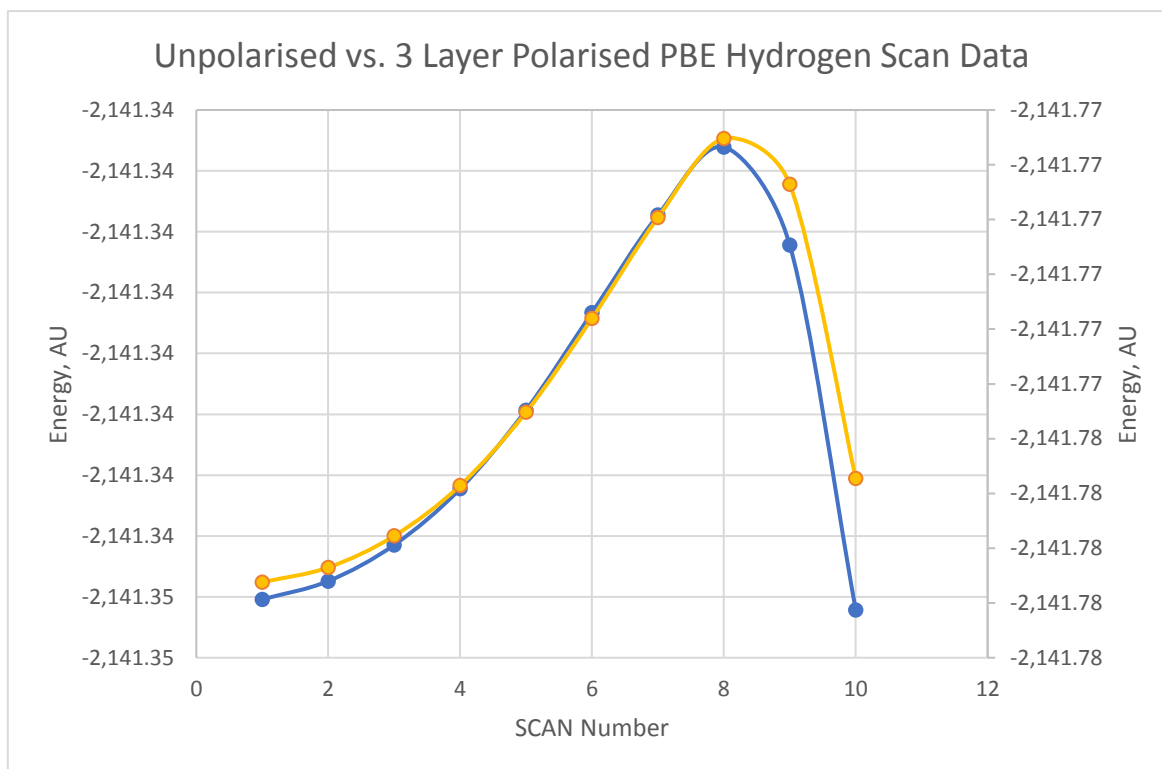


**Figure 11 - The unpolarised hydrogen scan energies against the hydrogen scan energies that have three layers of polarisation applied. This is done to show that similar energy curves are formed for the two systems which are the least similar. The three-layer polarised system is the yellow curve and is plotted against the secondary axis. TOLINTEG: 6 6 6 6 12, SHRINK: 2 2, TOLDEE: 8**

The scans presented in Fig. 10 show that the  $E_{\text{final}}$  is of higher energy than the  $E_{\text{initial}}$  in all instances apart from the unpolarised system. The  $E_{\text{final}}$  is the energy of the terminated system and atomic H whilst  $E_{\text{initial}}$  is the energy of the radical system and the  $\text{H}_2$ . For all systems that have polarisation applied, the curves show agreement with Cheesman et al.<sup>4</sup> who cite the energy of the radical system as  $0.7 \text{ kJ mol}^{-1}$  less energetic than the terminated system. Whilst there is an agreement between the data presented in Fig. 10 and Cheesman et al., the data collected in this thesis has a greater difference than that quoted by Cheesman et al. This thesis found that the radical system was less energetic, with a difference of  $2.70$ ,  $4.04$  and  $4.97 \text{ kJ mol}^{-1}$  for the one-, two-, and three-layer systems respectively. The unpolarised system shows an inaccurate value to that of the literature, with the radical system more energetic than the terminated system by  $4.55 \text{ kJ mol}^{-1}$ .

This shows that as more polarisation is applied, the energy difference between the two systems, increases. This was not stated in Cheesman et al.'s study. However, they modelled a cluster of diamond employing 6-311G\*\*/B3LYP, whilst this thesis employs periodic boundary conditions, which is more accurate, with less accurate basis set and functional. This may indicate why there is a deviation from the literature.

## Energy Barrier of Hydrogen Adsorption

Cheesman et al.<sup>4</sup> found the energy barrier to the H abstraction and H adsorption reaction to the (100) dimer carbon to be 26.4 kJ mol<sup>-1</sup> and 27.1 kJ mol<sup>-1</sup> respectively. They used a larger basis set, the 6-311G\*\*, whilst this thesis employed the 6-31G basis set. These values are in good agreement with Kang and Musgrave's<sup>20</sup> finding, who cited the abstraction value to equal to 28.5 kJ mol<sup>-1</sup>. Whilst both papers used the B3LYP functional and the same basis set, Cheesman et al. did not have to extrapolate their data to produce an accurate result, unlike Kang and Musgrave. Furthermore, Cheesman et al. provide a value for the adsorption reaction also. These reasons have led to the use of Cheesman et al.'s values as the literature that will be compared to.

*Table 5 - Energy barrier data to both the H adsorption and H abstraction for the different degrees of polarisation applied, calculated using the 6-31G/PBE-D3.*

Degree of Polarisation	PBE-D3 Energy Barrier Data, kJ mol <sup>-1</sup>	
	H Adsorption	H Abstraction
Unpolarised	11.98	10.34
One Layer	9.70	10.28
Two Layers	13.61	12.81
Three Layers	13.90	12.05

From the PBE-D3 (DFT) results, it is observed that applying polarisation increases the energy barrier to the adsorption reaction, making the value more accurate when compared to the values calculated by Cheesman et al.<sup>4</sup> However, the increase in accuracy whilst gradual, is very small. Generally, the approximated energy barrier for the H abstraction reaction also becomes more accurate to that of the literature value of 26.4 kJ mol<sup>-1</sup>.<sup>4</sup> However, there are anomalies in the results, with the PBE-D3 functional producing an energy barrier for the one-layer H adsorption reaction as well as the three-layer H abstraction that does not fit the expected trend.

The increase in accuracy of the H adsorption energy barrier between the two- and three-layer system, is calculated as 1.07 %. Regarding the H abstraction energy barrier, applying an extra layer of polarised carbons to the two-layer system leads to a decrease in accuracy of 2.88 %. This, coupled with the data in Table 7, allows for conclusions to be made. The increase in total calculation time required between the two- and three-layer systems is found to be 12.32 hours per node. Furthermore, the literature cites the energy difference between the H abstraction and H adsorption energy barriers to be - 0.7 kJ mol<sup>-1</sup>, which the two-layer system reproduces most convincingly.

Considering the statements above, the most suitable degree of polarisation for PBE calculations may be the two-layer polarised construction as this system produces the most accurate energy barrier values whilst not being the most expensive.

The reason as to why both the one-layer and unpolarised systems have been disregarded from this conclusion is due to several reasons. Firstly, the one-layer system produces results that mean the H adsorption reaction is less energetic than the H abstraction reaction. This disagrees with the literature cited by Cheesman et al. and therefore is not suitable when approximating the energy barriers of both the forward (adsorption) and reverse (abstraction) reactions. In addition, the unpolarised system produces values that are less accurate than both the two- and three-layer systems, with percentage errors of 60.8 and 55.80 % for the H abstraction and adsorption barriers respectively.

The PBE-D3 functional has underestimated the energy barrier for the one-layer system so much that it no longer fits the trend shown by the rest of the data in Table 5. Using the data in Fig. 9, the energy causing the outlying data can be found. Both the energy of the terminated and radical systems calculated by PBE-D3 are within the trend observed in the figure. Therefore, the calculation must have underestimated the energy of the transition state, producing a smaller value overall from Eq. 1 and 2. The reasons for the underestimation of the TS are unclear, but given more time, rerunning the H scan or optimising the TS geometry of the one-layer system may solve this.

Overall, the degree of error in the presented energy barriers are expected, as studies such as Kang and Musgrave in 2000,<sup>20</sup> used a more sophisticated computational approach (6-31G\*\*/B3LYP) compared to this thesis and produced data that showed an error of 39.77 %. After manipulation and extrapolation of this value using external H abstraction processes, they produced a value of 28.45 kJ mol<sup>-1</sup>, which has an error of 7.77 % when compared to the value presented more recently by Cheesman et al.<sup>4</sup> Using the method they employed to find the energy barrier of the H abstraction reaction, the data seen in Table 6 is produced.

**Table 6 - Energy barrier data of the H abstraction reaction produced using the method from Kang and Musgrave (2000). They found their 6-31G\*\*/B3LYP method underestimated the barrier by 13 kJ mol<sup>-1</sup>. They found this by applying the method to estimate the H abstraction energy barrier to ethane. They experimentally knew this value and added the difference to the energy barrier found from the dimer reconstructed diamond system.**

Degree of Polarisation	PBE-D3 Energy Barrier Data, kJ mol <sup>-1</sup>	
	H Abstraction	H Abstraction using Kang and Musgrave Extrapolation
Unpolarised	10.34	23.34
One Layer	10.28	23.28
Two Layers	12.81	25.81
Three Layers	12.05	25.05

From the data produced by this thesis, coupled with the extrapolation method presented by Kang and Musgrave, the error in the data significantly decreases and the data agrees very closely with the

26.4 kJ mol<sup>-1</sup> energy barrier presented by Cheesman et al.<sup>4</sup> The two-layer system most closely agrees with the literature, with a percentage error of only 2.23 %. Taking this approach from Kang and Musgrave is a very effective way of reproducing data from the literature, although it cannot be used build upon previous values or argue for a different value of the abstraction energy barrier.

### B3LYP Single-point Data

*Table 7 - Single-point energy calculations of the terminated layers, radical and TS systems. The calculations used 6-31G/B3LYP.*

Degree of Polarisation	B3LYP-D3 Single-point Energy, AU		
	Terminated	Radical	Transition State
Unpolarised	-2142.0464	-2141.3786	-2142.5097
One-Layer	-2142.2259	-2141.5568	-2142.6874
Two-Layer	-2142.3830	-2141.7143	-2142.8450
Three-Layer	-2142.5455	-2141.8772	-2143.0080

Table 7 presents data that corroborates the claim that polarisation reduces the energy of the reconstructed diamond system as well as the TS of the adsorption/abstraction reaction. This can be seen in the regular decrease of each systems energy as more polarisation is applied. In each system, the application of polarisation to three layers of carbon atoms (as well as the top layer of hydrogen atoms) results in a reduction of around 0.5 AU. This difference is almost identical throughout the systems presented in this thesis. Crucially, by collecting this data allowed for a broad estimate of the B3LYP calculated energy barriers of both the H adsorption and abstraction reactions.

*Table 8 - Formed using the data from Table 7. The barriers were calculated using Eq. 1 and 2 also. The H and H2 values were calculated using B3LYP also and have values of -0.496862 and -1.169590 AU respectively.*

Degree of Polarisation	B3LYP Energy Barriers, kJ mol <sup>-1</sup>	
	H Adsorption	H Abstraction
Unpolarised	101.29	88.11
One-Layer	102.32	92.72
Two-Layer	102.06	91.37
Three-Layer	101.95	90.37

Whilst the data in Table 8 presents energy barrier values that are not in agreement with Cheesman et al. they do show how polarisation effects the energy barriers of both reactions. Generally, the energy barriers change most when any form of polarisation is applied to the unpolarised system. The energy barrier does not deviate much between systems that already have polarisation applied to them. This can be seen by the difference of just 0.37 and 2.35 kJ mol<sup>-1</sup> for the adsorption and abstraction reactions respectively, between the polarised systems. The PBE data also suggests this as there is only a

difference of 1.92 and 1.71 kJ mol<sup>-1</sup> between the unpolarised and three-layer PBE adsorption and abstraction energy barriers respectively. This supports the use of less or no polarisation, as a compromise between the accuracy of the data and computational cost.

The inaccuracy of the data in Table 8 is not much of concern. This is because they are single-point calculations taken using the B3LYP functional of geometries that were produced by the less accurate PBE-D3 functional. Therefore, the values are not going to be accurate, although still show the minor difference polarisation makes to the energy barrier values.

## Computational Runtime

*Table 9 - CPU Runtime per node in node hours, taken from the OUTPUT files of hydrogen scan energies of the adsorption reaction. The time is the total time to calculate the system's energy, including the SCF convergence and the optimisation of the structure.*

Degree of Polarisation	H-Scan Runtime, CPU Time
	PBE-D3
Unpolarised	420.32
1 Layer	456.09
2 Layers	553.16
3 Layers	565.48

Using the data from both Tables 5 and 9, conclusions about the effectiveness of applying polarisation to the H adsorption reaction can be made. The CPU runtime consecutively increases, although not by much, as more polarisation is applied to the diamond structure, which is expected as more polarisation needs to be accounted for in the geometry optimisations. This can be seen in both the calculations using PBE-D3 and the B3LYP functionals. The most accurate surface reconstruction of diamond modelled using PBE, in theory, is the system with three layers of polarisation applied and the least accurate is the unpolarised system. The increase in computational run time between these two systems is 145.16 hours, which results in a percentage error reduction of 6.4576 %.

Whilst it is stated above that the PBE-D3 functional gives a good estimation of the H adsorption, with a 27.4% error to that of the literature, it may be more economically viable to apply less or even no polarisation despite the increase in error. By reducing the polarisation applied to the system by a layer (eight atoms), the percentage error increases from 27.4 to 28.8%. However, the CPU runtime is reduced by 12.32 hours per node. In these calculations, four nodes were used, therefore resulting in a total reduction of 49.28 hours to only get a achieve a value 1.4% more accurate. These conclusions should be taken into consideration when calculating energy barrier calculations of surface reactions of large systems such as diamond.

**Table 10 - CPU runtime for both the SCF convergence and optimisation of the c-radical structure from a polarised terminated (100) - 2x1 dimer reconstruction. Both the PBE-D3 and B3LYP functional have been used to produce these values. One node has 28 cores.**

Degree of Polarisation	C-radical Runtime, CPU Time	
	PBE-D3	B3LYP
Unpolarised	31.72	55.24
1 Layer	33.86	64.80
2 Layers	43.90	92.53
3 Layers	46.99	68.41

## Functional Runtime

**Table 11 - TELAPSE data showing the hours per node required to calculate the converged self-consistent field during the hydrogen scanning calculations attempting to find the energy of the transition state. This was an alternative way to compare the cost of using both the PBE-D3 and B3LYP functionals.**

Degree of Polarisation	H-SCAN TELAPSE Data	
	PBE-D3	B3LYP
Unpolarised	3.76	5.90
One Layer	4.08	-
Two Layer	4.94	-
Three Layer	5.05	-

It should be noted that the lack of B3LYP H-Scan data is due to the B3LYP functional not optimising the geometry system during the H-Scan calculations. Despite this, strong conclusions can still be made concerning the functionals. From the data in Table 11, we can clearly see that as polarisation is applied, the time required for the SCF to converge regularly increases. Furthermore, the time needed for the B3LYP to converge the SCF for an unpolarised system is greater than the time required for the SCF of a system with three-layers (32 atoms) to be converged. This highlights what was already believed, as the more complex B3LYP functional requires more time to calculate the same systems in the hope of increased accuracy.

The extra time required for the convergence of the unpolarised system's SCF was 56.9 %. It should be noted, these times are negating the time for optimisation of the geometry, and therefore the B3LYP functional may require even more computational time to calculate the system's geometry. This highlights the requirement for cheaper computational methods, which can either be parameterised or reliably extrapolated. Whilst it is safe to assume that as more atoms are polarised, the B3LYP calculation would require more time to calculate the SCF, extrapolation of the data to estimate the time required is not appropriate as more data points are required.

## Geometry Observations

### Terminated and C-Radical Differences

In the diagrams below, a face-on view and a side profile of the (2x1) reconstructed dimer bond can be seen in Fig. 12. In Fig 13., the same perspectives of the radical dimer carbon are depicted. Both angles and bond lengths are being evaluated in the results.

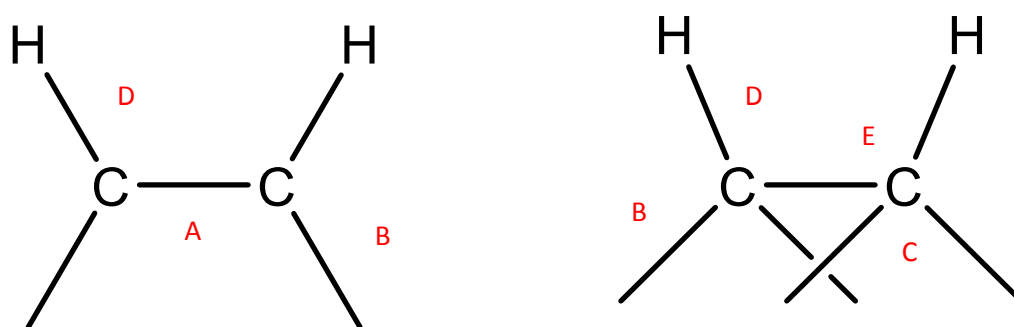


*Figure 12 - Terminated Dimer Bond Depictions from ChemDraw. A is the dimer bond length. B is the interlayer bond length, specifically the bond length between the dimer carbon and the neighbouring carbon in the second layer of the terminated system. C is the angle between the dimer carbon and the two neighbouring carbons in the second layer. D is the bond length between the dimer carbon and the terminating hydrogen. E is the angle between the dimer bond and the terminating hydrogen.*

*Table 12 – Geometry data concerning the terminated dimer system.*

Polarisation Applied	Terminated Dimer Reconstruction Geometry Data									
	(A) Dimer Bond Length, Å		(B) Interlayer Bond Length, Å		(D) C-H Bond Length, Å		(E) C-C-H Bond Angle, °		(C) C-C <sub>term</sub> -C Bond Angle, °	
	PBE-D3	B3LYP	PBE-D3	B3LYP	PBE-D3	B3LYP	PBE-D3	B3LYP	PBE-D3	B3LYP
Unpolarised	1.64	1.64	1.56	1.56	1.11	1.10	112.6	112.6	111.3	111.4
1 Layer	1.63	1.63	1.56	1.56	1.11	1.10	112.6	112.5	111.4	111.4
2 Layers	1.63	1.63	1.56	1.56	1.11	1.10	112.6	112.5	111.5	111.4
3 Layers	1.63	1.63	1.56	1.56	1.11	1.10	112.6	112.5	111.6	111.4

From Table 12, applying polarisation to the system reduces the dimer bond (A) by 0.01 Å from 1.64 Å to 1.63 Å. There is perfect agreement between the geometries calculated by the PBE-D3 and B3LYP functionals. The minute change may not be very significant, but it does show that the bond becomes minorly stronger after polarisation is applied. Furthermore, the dimer bond length does not change after the first layer of polarisation is applied. This may infer that polarisation to the layers that are not the surface (the layer containing the dimer system) will not further affect this bond. This is a sensible

observation as polarisation to the surface atoms is unlikely to affect a bond that is parallel with the surface.

The only major difference in the geometric results produced by the two functionals can be seen in the C-C<sub>term</sub>-C bond angle, in Table 12.C. The PBE-D3 functional calculates an increasingly obtuse angle as a higher degree of polarisation is applied. This infers that the two dimer carbons relax slightly into the lattice as high degrees of polarisation is applied. Although, this value does not change when the geometry is optimised by the B3LYP and therefore the dimer carbon does not sit closer into the lattice, assuming the B3LYP functional is more accurate.

Furthermore, the B3LYP functional calculates the C-H bond to be 1.10 Å which is 0.01 Å shorter than the value calculated by PBE-D3. Kang and Musgrave<sup>20</sup> cite the C-H bond as 1.09 Å, implying the B3LYP calculates a more accurate value of the C-H bond. In addition, Kang and Musgrave also calculated a dimer bond value on 1.63 Å, which is correctly calculated by both PBE-D3 and B3LYP ensuring polarisation is applied to the system. The minor difference between the B3LYP and the literature values may be due to the 6-311G\*\* basis set they used.

Kang and Musgrave<sup>20</sup> found the bulk diamond bond length to be 1.54 Å. This is in good agreement with the bulk diamond bond length calculated in this thesis as 1.52 Å. However, this thesis found the bulk bond length to be 1.52 Å regardless of the functional used or the polarisation applied to the system. Considering this, the difference between the bulk diamond bond length and the calculated dimer bond length from Table 12 is even larger than that cited in Kang and Musgrave. This thesis cites the difference of these two lengths as 0.11 Å, compared to the difference in Kang and Musgraves<sup>20</sup> paper of 0.05 Å, indicating the degree of strain may be greater than what was previously believed. Furthermore, the dimer bond length of the terminated system is already smaller than the van der Waals radii for carbon, cited as 1.7 Å.<sup>59</sup>

The only geometric measurement that the PBE-D3 inconsistently calculated is the angle between the dimer carbon and the two carbons in the second layer of the lattice, seen as Fig. C. The PBE-D3 calculated angle varied depending on the polarisation applied, whereas the B3LYP calculated angle was consistent regardless of the polarisation applied. As each layer of polarisation is applied, the angle increases by 0.1 °. This results in a change of 0.3 ° between the angle in the unpolarised and three-layer system. This seems to imply that the dimer carbons relax slightly further into the crystal as more polarisation is applied.

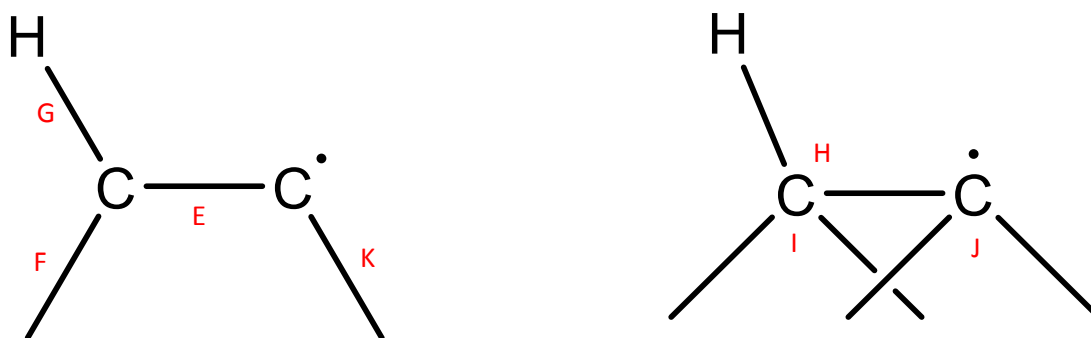


Figure 13 - Radical Dimer Bond from ChemDraw, E is the dimer bond length. F is the terminated interlayer bond length. K is the radical interlayer bond length. H is the angle between the dimer bond and the terminated hydrogen. I is the angle between the terminated dimer carbon and the second layer carbons. J is the bond between the radical dimer carbon and the two carbons in the second layer of the radical system.

Table 13 - Geometry data concerning the c-radical system.

Polarisation Applied	Radical Dimer Reconstruction Geometry Data											
	(E) Dimer Bond Length, Å		(F) Terminated Interlayer Bond Length, Å		(G) C-H Bond Length, Å		(H) C-C-H Bond Angle, °		(I) C-C <sub>term</sub> -C Bond Angle, °		(J) C-C <sub>radical</sub> -C Bond Angle, °	
	PBE-D3	B3LYP	PBE-D3	B3LYP	PBE-D3	B3LYP	PBE-D3	B3LYP	PBE-D3	B3LYP	PBE-D3	B3LYP
Unpolarised	1.61	1.61	1.57	1.56	1.11	1.09	115.3	115.3	111.2	111.6	114.6	114.7
1 Layer	1.60	1.60	1.57	1.57	1.11	1.1	115.3	115.2	111.3	111.3	114.7	114.7
2 Layers	1.60	1.60	1.56	1.56	1.11	1.1	115.4	115.3	111.5	111.4	114.9	114.8
3 Layers	1.60	1.60	1.56	1.56	1.11	1.1	115.3	115.3	111.5	111.5	114.9	114.9

In all cases of applied polarisation, the dimer bond shortens, with the largest change of 0.03 Å occurring in the unpolarised system and where three layers of polarisation have been applied. This agrees with the Cheesman et al.'s<sup>4</sup> observations that the abstraction process results in a radical structure and this is slightly less energetic than the terminated dimer reconstruction. This is further supported by the shortening in dimer bond length after abstraction, strengthening the bond.

Furthermore, there is some discrepancy between the dimer bond length observed and the value from the literature. Kang and Musgrave<sup>20</sup> cite this value at 1.59 Å, which is in contrast with the observed dimer bond length as 1.63 Å. The difference between these values may be due to the difference in the model structure. This thesis employs periodic boundary conditions, with a single cell comprising of 72 carbon atoms, whereas Kang and Musgrave<sup>20</sup> employed a cluster of 37 carbon atoms. Therefore, this thesis potentially produces more accurate dimer bond lengths despite the employment of a smaller basis set when compared to Kang and Musgrave.

In addition, the Kang and Musgrave calculated the interlayer C-C bond length of diamond to be equal to 1.54 Å. This is in good agreement with the calculated interlayer C-C bond length of 1.56 Å, which is

seen in Table 12. The value of the C-H dimer bond length was calculated as 1.09 Å by Kang et al.<sup>20</sup>, which also corroborates the calculated C-H bond length of 1.11 Å. This value is the same despite the degree of polarisation applied.

Further observations showed that the symmetry between the two carbons in the dimer bond is removed after the abstraction of the dimer H occurs. This can be specifically seen in the change in geometric parameters of the two dimer carbons. Firstly, there is a change in the interlayer bond length of both dimer carbons, with the terminated carbon (the left carbon on Fig. 13) bond length elongating by 0.01 Å, from 1.56 Å to 1.57 Å. In addition, when H abstraction occurs the interlayer bond length shortens slightly from 1.56 Å to 1.53 Å, indicating the bond becomes marginally stronger.

These observations, coupled with the C-C<sub>radical</sub>-C angle becoming more obtuse after H abstraction, results in the radical carbon relaxing more into the crystal lattice. In contrast, the C-C<sub>terminated</sub>-C bond angle becomes more acute. The smallest change in radical bond angle is seen in the one-layer system, with all the others having equal changes of 3.4°. Another observation to note is that as the polarisation applied to the system increases, the more obtuse the dimer C-C-C bond angle becomes. The unpolarised system has an angle of 111.1° which increases to 111.4° after two layers of polarisation has been applied. This implies the dimer carbons sit closer into the lattice once polarisation is applied.

Regarding the slightly larger lattice parameter applied to the 6-31G/B3LYP, the minute change in the value has not seemed to translate to the geometry of both the terminated and radical systems. The larger lattice parameter would suggest that the B3LYP calculated crystal would have marginally longer bonds. This was not observed in the dimer bond of either of the systems, although JMOL only quotes the bond lengths to 0.01 Å, and therefore the difference may not be observed.

From the data in Tables 12 and 13, it can be concluded that the 6-31G/PBE-D3 method produces a system that is geometrically in good agreement with the 6-31G/B3LYP system. Whilst the starting and final structure of the H adsorption reaction are important, analysing the geometry of the TS is critical to make definite conclusions on concerning the use of the B3LYP or PBE-D3 functionals.

### Transition State Geometry

It should be noted that the transition states are approximations and therefore their geometry should be approached with caution. The method to make these approximations more accurate shall be discussed in the section concerning future work.

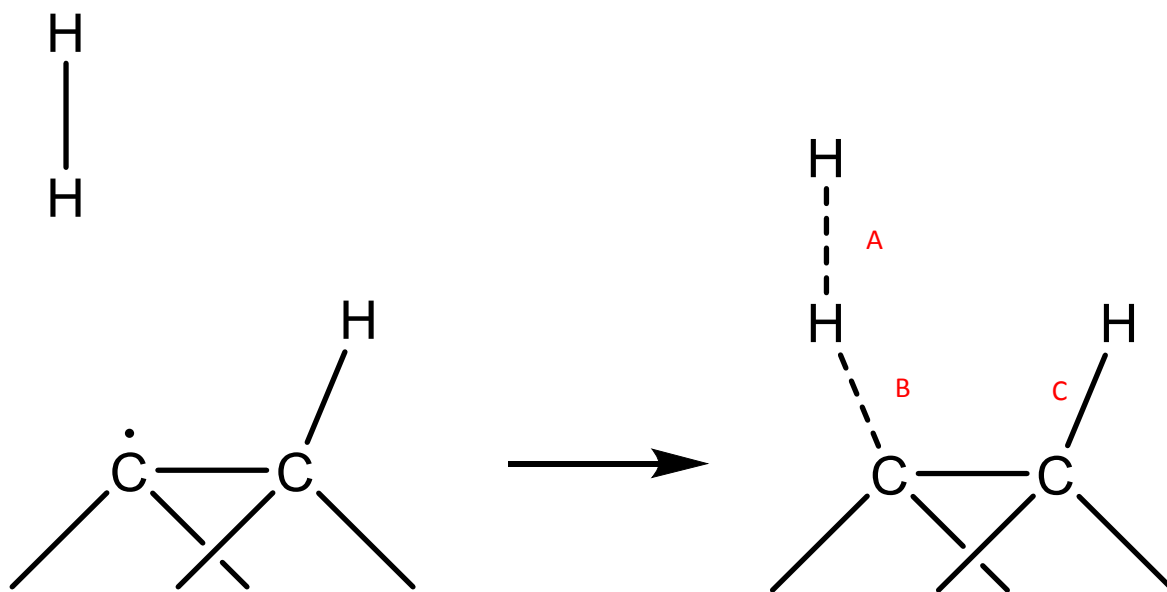


Figure 14 - Depiction of the TS of the H adsorption/abstraction reaction regarding the (100) dimer surface reconstruction of diamond. Dashed bonds are partial bonds.

Table 14 - Transition state geometry, including the H-H partial bond length, the C-H partial bond length and the bond angle between the dimer bond and the neighbouring terminated H.

PBE-D3 Transition State Geometry				
	H-H Bond Length, Å (A)	C-H Bond Length, Å (B)	Neighbouring C-C-H Bond Angle at $E_{TS}$ , ° (C)	C-C-H Bond Angle at $E_{final}$ , ° (D)
Unpolarised	1.05	1.33	113.9	112.3
1	1.06	1.33	113.8	112.4
2	1.05	1.33	113.9	112.4
3	1.05	1.33	113.9	112.3

When comparing the data in Table 14 there is not much deviation caused between the values/presented when applying higher degrees of polarisation. However, by using the output file and the necessary scan file, which in all cases was SCAN 8 in Fig. 10, the transition state geometry can be found. By animating the H adsorption process and freezing it at the necessary scans, the transition state of each system produces the data in Table 14. At the transition state, the partial bond length of the H-H is seen as 1.05 Å. However, this value is potentially unreliable due to the starting H<sub>2</sub> bond length being set to 0.8 Å rather than 1.0 Å to ensure bonding. Therefore, this value may be an underestimation of the TS H-H bond length.

Furthermore, using the data from Table 13 and 14, at the transition state the bond angle between the dimer bond and the neighbouring H atom to the c-radical increases. For example, in the three layers system, the angle increases from 111.5 ° to 113.9 ° from the c-radical to the TS. This implies the

neighbouring H moves slightly away from the incoming H atom. This could be due to the increased steric repulsion as the H moves towards the TS. Also, the increased interactions between the neighbouring atoms increase, which results in the increased energy of the system also. This bond angle then relaxes to an angle of  $112.3^\circ$  once the radical has been terminated.

From the data in Table 14, the H-H partial bond is minorly stronger as more polarisation is applied, whilst the distance between the carbon radical and the bonding H remains constant. The change in the angle is so minute that more investigation into the TS geometry must be made to make justified conclusions.

Overall, clear and defining conclusions regarding the effect of polarisation on the TS geometry cannot be made. From the geometric data shown above, it can be concluded that there is little geometric difference between the B3LYP and PBE calculated structures when further polarisation is applied. Despite this, the energy of the TS does drop considerably as more polarisation is introduced.

## Limitations of the Thesis

At the start of the thesis, the researcher was a novice at both coding and the use of Linux. By the end of the data collection, the researcher became competent in the production of the necessary INPUT files and the contents. The author's learning curve was steep, and consequently, the efficiency that data was produced and collected was reduced due to this. Often, the programme would produce inaccurate OUTPUT files. Many of the mistakes were due to human error, whether a specific interaction or optimisation block were missing.

Whilst many of these issues were solved by the researcher, there were many occasions where advice and guidance were required. Furthermore, the lack of experience increased the time taken to collect the data, as jobs were put on the 'submission queue' to only produce incorrect results. Many jobs, especially the hydrogen scan calculations, can take up to two days to complete depending on the functional employed, which consequently resulted in lost time. In retrospect, attending a Linux, python or CRYSTAL17 course would have provided prior experience to ensure a better understanding of the tasks being undertaken, subsequently leading to a more efficient collection of the energy barrier data. Having prior python experience may have facilitated the production of useful scripts to aid in the collection of the necessary data from the OUTPUT files.

In addition, there were some issues with calculation jobs failing without INPUT error. These were usually due to node failures and was an issue that would be specific to a node. The only problem these occurrences caused was the loss of time, and with some calculations taking up to two days, there were

instances of a lot of lost time. Whilst this was out of the researcher's control, it was still a limitation to the data collection and could only be addressed by notifying the necessary people for further support.

### B3LYP Optimisation

There were numerous instances of problems with the B3LYP functional calculations. The issues stemmed from the geometry optimisation of the system, which would not converge and would either carry out the maximum number of cycles allowed or reach the time limit allowed for calculation, both resulting in errors and unfinished calculations.

This resulted in the compromise of taking single-point energies of each system, which can be seen above in Table 7. Whilst this approach meant that no data regarding the TS of the adsorption/abstraction reaction was found, it did produce the necessary energy values required to approximate the energy barrier values of both reactions. Furthermore, it allowed for the SCF convergence runtime to be evaluated for both the PBE and B3LYP functionals.

This was very unfortunate, as obtaining the B3LYP calculated TS would have provided this thesis with very comparable, interesting data. From this, more solid conclusions could be made on the degree of polarisation necessary for modelling surface reactions on the diamond reconstruction.

### Further Studies

With the experience the researcher now has of the methodology, there are areas of surface reactions of (100) dimer surface that could be investigated. Clusters of polarisation could be included in the research, in order to investigate whether a cluster of polarisation around the reaction zone produces similar data to the one- or two-layer systems, potentially reducing the computational run costs further. This would be interesting as this thesis shows that applying polarisation to additional layers does not affect the energy barriers very much. Therefore, applying polarisation to a cluster around the reaction area may cause greater increases in accuracy. This would also answer whether a cluster of atoms surrounding the reacting dimer bond requires polarisation to affect its geometry.

Furthermore, it would have been worth conducting fine scans of the transition state of all degrees of polarisation. To do this, the same method would be carried out, but the starting position of the hydrogen molecule would be closer to the TS. Doing this would produce more accurate values of the TS for those functionals and therefore result in more accurate barrier values. The reason this was not done in this thesis, was to ensure computational costs were kept to a minimum, emphasising whether the literature could be reliably reproduced using methods that led to the lowest cost.

In addition, the use of larger and smaller basis sets and keeping the functional would be quite an interesting approach. Not only would this show which basis set is the most accurate for the corresponding functional but collecting the CPU time would also present which basis set is most suitable for these types of calculations. This data could be used for later research concerning diamond surface reactions.

A key requirement for future study is to test the accuracy of calculating the H adsorption and H abstraction barriers. This would solidify the arguments presented for the validity of using DFT functionals to approximate energy barriers in large, computationally expensive systems. Furthermore, it would determine whether the energy value of the terminated system calculated using 6-31G/B3LYP is indeed an anomaly.

## Conclusion

In conclusion, this thesis has presented arguments in favour of the use of DFT functionals to approximate energy barriers of surface reactions of the reconstructed diamond surface. In conjunction, it has presented methods to reduce the cost of calculation depending on the system being investigated.

When researching the simple surface reactions such as the H adsorption and abstraction reactions of diamond, the data presented suggests the use of little to no polarisation and polarising the whole system is not appropriate due to the vast increase in computational power used. Furthermore, the thesis presents the use of two-layer system as a nice compromise between accuracy and runtime. However, the addition of polarisation to the system does not add much agreement to the energy barrier values with the literature and therefore it may be viable to not add polarisation at all. This would further reduce the cost of the calculations.

Furthermore, the thesis shows that employing small basis sets and cheaper functionals (6-31G/PBE-D3) leads to a consistent approximations of both energy barriers that can then be used in further calculations. Also, using extrapolation methods, such as the approach presented by Kang and Musgrave<sup>20</sup>, a more accurate value of the H abstraction energy barrier can be obtained. Moreover, after extrapolation, the energy barrier to the abstraction estimated is even more accurate to recent literature by Cheesman et al.<sup>4</sup> This is despite Kang and Musgrave<sup>20</sup> using a much more accurate method (6-31G\*\*/B3LYP). This may have been achieved due to the periodic boundary conditions employed in this thesis.

Overall, this thesis has aimed to demonstrate that the use of DFT functionals absolutely is a viable method to estimate the energy barriers of surface reactions concerning diamond CVD, especially when cost of calculation is being considered.

## References

- 1 *United States Pat. Off.*, 1962, **28**, 131–134.
- 2 T. Tohei, A. Kuwabara, F. Oba and I. Tanaka, *Phys. Rev. B*, 2006, **73**, 64304.
- 3 S. Skokov, B. Weiner and M. Frenklach, *J. Phys. Chem.*, 1994, **98**, 7073–7082.
- 4 A. Cheesman, J. N. Harvey and M. N. R. Ashfold, *J. Phys. Chem. A*, 2008, **112**, 11436–11448.
- 5 H. M. King, How Do Diamonds Form? | They Don't Form From Coal!, <https://geology.com/articles/diamonds-from-coal/>, (accessed 11 March 2020).
- 6 H. M. King, Diamond: A gem mineral with properties for industrial use, <https://geology.com/minerals/diamond.shtml>, (accessed 8 March 2020).
- 7 R. Abbaschian, H. Zhu and C. Clarke, *Diam. Relat. Mater.*, 2005, **14**, 1916–1919.
- 8 A. Gicquel, K. Hassouni, F. Silva and J. Achard, *Curr. Appl. Phys.*, 2001, **1**, 479–496.
- 9 M. Werner and R. Locher, *Reports Prog. Phys.*, 1998, **61**, 1665.
- 10 F. P. Bundy, *Science (80-. )*, 1962, **273**, 8–10.
- 11 J. C. Angus, H. A. Will and W. S. Stanko, *J. Appl. Phys.*, 1968, **39**, 2915–2922.
- 12 J. J. Lander and J. Morrison, *Surf. Sci.*, 1966, **4**, 241–246.
- 13 D. N. Belton and S. J. Schmieg, *Surf. Sci.*, 1990, **233**, 131–140.
- 14 A. Netto and M. Frenklach, *Diam. Relat. Mater.*, 2005, **14**, 1630–1646.
- 15 P. W. May, *R. Soc.*, 2000, **358**, 473–595.
- 16 S. Matsumoto, *J. Mater. Sci.*, 1985, **4**, 600–602.
- 17 M. Kamo, Y. Sato, S. Matsumoto and N. Setaka, *J. Cryst. Growth*, 1983, **62**, 642–644.
- 18 S. Matsumoto, Y. Sato, M. Kamo and N. Setaka, *Jpn. J. Appl. Phys.*, 1982, **21**, L183
- 19 S. Matsumoto, Y. Sato, M. Tsutsumi and N. Setaka, *J. Mater. Sci.*, 1982, **17**, 3106–3112.
- 20 J. K. Kang and C. B. Musgrave, *J. Chem. Phys.*, 2000, **113**, 7582–7587.
- 21 T. J. Kistenmacher, S. A. Ecelberger and B. R. Stoner, *Diam. Relat. Mater.*, 1995, **4**, 1289–1295.
- 22 P. W. May, J. N. Harvey, N. L. Allan, J. C. Richley and Y. A. Mankelevich, *J. Appl. Phys.*, 2010, **108**, 114909.
- 23 nucleation | Definition, Crystallization, & Facts | Britannica, <https://www.britannica.com/science/nucleation>, (accessed 13 March 2020).
- 24 B. V. Spitsyn, L. L. Bouilov and B. V. Derjaguin, *J. Cryst. Growth*, 1981, **52**, 219–226.
- 25 P. K. Bachmann, D. Leers and H. Lydtin, *Diam. Relat. Mater.*, 1991, **1**, 12.

- 26 J. J. Gracio, Q. H. Fan and J. C. Madaleno, *J. Phys. D. Appl. Phys.*, 2010, **43**, 374017.
- 27 J. C. Angus, *Diam. Relat. Mater.*, 2014, **49**, 77–86.
- 28 P. W. May, J. N. Harvey, J. A. Smith and Y. A. Mankelevich, *J. Appl. Phys.*, 2006, **99**, 1–11.
- 29 E. J. Corat, N. G. Ferreira, N. F. Leite and V. J. Trava-Airoldi, *Mater. Res.*, 2002, **6**, 63–70.
- 30 B. Garrison, E. Dawnkaski, D. Srivastava and D. Brenner, *Science (80-. )*, 1992, **255**, 835–838.
- 31 S. J. Harris and D. G. Goodwin, *J. Phys. Chem.*, 1993, **97**, 23–28.
- 32 J. D. Kubicki, W. F. Bleam, J. R. Rustad, D. A. Dixon, N. T. Skipper, R. T. Cygan, E. Tipping, J. D. Kubicki and W. F. Bleam, *An Introduction to Molecular Modeling*, 2015.
- 33 E. G. Lewars, *Computational chemistry: Introduction to the theory and applications of molecular and quantum mechanics: Third Edition 2016*, 2016.
- 34 W. Kohn and L. J. Sham, *Phys. Rev.*, 1965, **140**, A1133–A1138.
- 35 P. J. Stephens, F. J. Devlin, C. F. Chabalowski and M. J. Frisch, *J. Phys. Chem.*, 1994, **98**, 11623–11627.
- 36 S. Salustro, F. Pascale, W. C. Mackrodt, C. Ravoux, A. Erba and R. Dovesi, *Phys. Chem. Chem. Phys.*, 2018, **20**, 16615–16624.
- 37 R. Dovesi, V. R. Saunders, C. Roetti, R. Orlando, F. Pascale, B. Civalleri, K. Doll, N. M. Harrison, I. J. Bush, P. D. Arco, M. Llunel and M. Caus, .
- 38 J. C. Richley, J. N. Harvey and M. N. R. Ashfold, *J. Phys. Chem. A*, 2009, **113**, 11416–11422.
- 39 A. D. Becke, *J. Chem. Phys.*, 1993, **98**, 1372–1377.
- 40 C. Lee, W. Yang and R. G. Parr, *Phys. Rev. B*, 1988, **37**, 785–789.
- 41 C. Adamo and V. Barone, *J. Chem. Phys.*, 1999, **110**, 6158–6170.
- 42 J. P. Perdew, M. Ernzerhof and K. Burke, 1996, **9982**, 9982–9985.
- 43 M. Andersen, C. Panosetti and K. Reuter, *Front. Chem.*, 2019, **7**, 1–24.
- 44 B. Meng and W. H. Weinberg, *Surf. Sci.*, 1996, **364**, 151–163.
- 45 W. J. Rodgers, P. W. May, N. L. Allan and J. N. Harvey, *J. Chem. Phys.*, 2015, **142**, 214707.
- 46 J. S. Foord, K. P. Loh and R. B. Jackman, *Surf. Sci.*, 1998, **399**, 1–14.
- 47 S. Skokov, B. Weiner and M. Frenklach, *J. Phys. Chem.*, 1994, **98**, 8–11.
- 48 S. Skokov, B. Weiner and M. Frenklach, *Phys. Rev. B*, 1994, **49**, 11374–11382.
- 49 S. Skokov, C. S. Carmer, B. Weiner and M. Frenklach, *Phys. Rev. B*, 1994, **49**, 5662–5671.
- 50 H. Tamura, H. Zhou, Y. Hirano, S. Takami, M. Kubo, R. V. Belosludov, A. Miyamoto, A. Imamura, M. N. Gamo and T. Ando, *Phys. Rev. B - Condens. Matter Mater. Phys.*, 2000, **62**, 16995–17003.
- 51 J. E. Butler, A. Cheesman and M. N. R. Ashfold, in *CVD Diamond for Electronic Devices and Sensors*, John Wiley & Sons, Ltd, Chichester, UK, 2009, pp. 103–124.
- 52 E. I. Axelsson, K. Brezinsky, F. L. Dryer, W. J. Pitz and C. K. Westbrook, *Symp. Combust.*, 1988, **21**, 783–793.

- 53 I. I. Oleinik, D. G. Pettifor, A. P. Sutton and J. E. Butler, *Diam. Relat. Mater.*, 2000, **9**, 241–245.
- 54 P. W. May and Y. A. Mankelevich, *J. Appl. Phys.*, 2006, **100**, 1–9.
- 55 C. C. Battaile, D. J. Srolovitz, I. I. Oleinik, D. G. Pettifor, A. P. Sutton, S. J. Harris and J. E. Butler, *J. Chem. Phys.*, 1999, **111**, 4291–4299.
- 56 S. Matsumoto, Y. Sato and N. Setaka, *Carbon N. Y.*, 1981, **19**, 232–234.
- 57 R. Issaoui, J. Achard, F. Silva, A. Tallaire, V. Mille and A. Gicquel, *Phys. Status Solidi Appl. Mater. Sci.*, 2011, **208**, 2023–2027.
- 58 I. Grant, The Self-Consistent Field Method - Potential Energy Surfaces, <http://www.chm.bris.ac.uk/webprojects2002/grant/webcomp/scf.html>, (accessed 16 March 2020).
- 59 A. Bondi, *J. Phys. Chem.*, 1964, **68**, 441–451.